

Supporting Information

Photoluminescence and Electrochemiluminescence of Thermally Activated Delayed Fluorescence (TADF) Emitters Containing Diphenylphosphine Chalcogenide-Substituted Carbazole Donors

*Shiv Kumar,^{†,a} Pauline Tourneur,^{†b} Jonathan R. Adsetts,^{†,c} Michael Y. Wong,^a Pachaiyappan Rajamalli,^a Dongyang Chen,^a Roberto Lazzaroni,^{b,d} Pascal Viville,^d David B. Cordes,^a Alexandra M. Z. Slawin,^a Yoann Olivier,^{*e} Jérôme Cornil,^{*b} Zhifeng Ding^{*c} and Eli Zysman-Colman^{*a}*

^a Organic Semiconductor Centre, EaStCHEM School of Chemistry, University of St Andrews, St Andrews, Fife, UK, KY16 9ST; E-mail: eli.zysman-colman@st-andrews.ac.uk; URL: <http://www.zysman-colman.com>;

^b Laboratory for Chemistry of Novel Materials, University of Mons, Mons, Belgium; E-mail: Jerome.Cornil@umons.ac.be; URL: <http://morris.umons.ac.be/>;

^c Department of Chemistry, The University of Western Ontario, London, Ontario N6A 3K7, Canada; E-mail: zfding@uwo.ca; URL: <https://publish.uwo.ca/~zfding/>

^d Materia Nova, Materials R&D center, Mons, Belgium; Tel: +32 65 55 49 02; E-mail: Pascal.Viville@materianova.be; URL: <http://www.materianova.be/>

^e Unité de Chimie Physique Théorique et Structurale (UCPTS) & Laboratoire de Physique du Solide (LPS), Namur Institute of Structured Matter (NISM), University of Namur, Namur, Belgium; E-mail: yoann.olivier@unamur.be;

(†) Authors equally contributed.

Table of Contents

Experimental Section.....	S3
General synthetic procedures	S3
Photophysical measurements	S4
Electrochemical measurements:.....	S5
Theoretical modelling	S7
Synthesis	S7
TBDMS-PPCz.....	S7
PPOCz	S9
PPSCz.....	S9
PPOCzPN	S9
PPSCzPN.....	S10
TBDMS-DiPPCz.....	S11
DiPPOCz	S12
DiPPOCzPN	S12
Spectra	S14
X-Ray Crystallography	S34
Additional Electrochemical Experiments.....	S38
Theoretical modelling	S42
Electrochemiluminescence	S49
References.....	S54

Experimental Section

General synthetic procedures: All commercially available chemicals and reagent grade solvents were used as received. 3-Bromocarbazole, 3,6-dibromocarbazole, N-TBDMS-3-bromocarbazole and N-TBDMS-3,6-dibromocarbazole were prepared according to the literature.¹ Air-sensitive reactions were performed using standard Schlenk techniques under a nitrogen atmosphere. Anhydrous THF was obtained from a solvent purification system. Flash column chromatography was carried out using silica gel (60 Å, 40-63 µm). Analytical thin-layer-chromatography (TLC) was performed using silica plates with aluminum backings (250 µm with F-254 indicator), and were visualized using a 254/365 nm UV lamp. ¹H, ¹³C{¹H} and ³¹P{¹H} NMR spectra in CDCl₃ or DMSO-d₆ were recorded on an NMR spectrometer (400 MHz for ¹H, 101 MHz for ¹³C{¹H} and 162 MHz for ³¹P{¹H}). The NMR signal is described as follows: s = singlet, d = doublet, dd = doublet of doublets, td = triplet of doublets, ddd = doublet of doublets of doublets, and m = multiplets. Melting points were measured using open-ended capillaries on Electrothermal Mel-Temp® melting point apparatus and are uncorrected. High-resolution mass spectrometry (HRMS) was performed by the EPSRC National Mass Spectrometry Service Centre (NMSSC), Swansea University. Elemental analyses were performed by Mr. Stephen Boyer, London Metropolitan University. High performance liquid chromatography (HPLC) analysis was conducted on a Shimadzu Prominence Modular HPLC system. HPLC traces were performed using an ACE Excel 2 C18 analytical (3 × 150 mm) column. Gas chromatography mass spectrometry (GCMS) analysis was carried out on a Shimadzu GCMS-QP2010 SE instrument, an advanced standard gas chromatograph mass spectrometer coupled with automated AOC-5000 sample injection system using a Shimadzu-SH RTX®-1 column

(fused silica) (length = 25 m, inner diameter = 0.25 μm , oven temp.: 40 $^{\circ}\text{C}$ to 250 $^{\circ}\text{C}$; detector: MS; detection temp.: 250 $^{\circ}\text{C}$; Carrier gas: helium). The emitters **PPOCzPN** and **PPSCzPN** were each found to exist as a mixture of rotamers at room temperature in a ratio of 58:42 and 70:30, respectively, which was observed by both HPLC and $^{31}\text{P}\{^1\text{H}\}$ NMR spectroscopy. This was further substantiated by obtaining single crystals of both rotamers for **PPSCzPN**.

Photophysical measurements: Optically dilute solutions of concentrations on the order of 10^{-5} or 10^{-6} M were prepared in HPLC grade acetonitrile for absorption and emission analyses. Absorption spectra were recorded at room temperature on a Shimadzu UV-1800 double beam spectrophotometer. The molar absorptivity values were determined by linear regression analysis of four solutions of different concentrations within the range of 10^{-4} to 10^{-5} M prepared by dilution of stock solution (10^{-3} M). Aerated solutions were prepared by using aerated solvents with prior air bubbling for 5 min whereas degassed solutions were prepared *via* five freeze-pump-thaw cycles prior to emission analysis using a home-made cuvette with extended solvent bulb designed for cryogenic degassing. Steady-state emission and time-resolved emission spectra were recorded at 298 K using Edinburgh Instruments FLS980 fluorometer. Samples were excited at 360 nm using a Xenon lamp for steady-state measurements and at 378 nm using a PicoQuant pulsed diode laser for time-resolved measurements. Photoluminescence quantum yields for solutions were determined using the optically dilute method² in which four sample solutions with absorbance at 360 nm being ca. 0.10, 0.080, 0.060 and 0.040 were used. Their emission intensities were compared with those of a reference, quinine sulfate, whose quantum yield (Φ_r) in 1 N H_2SO_4 was taken as 54.6%.³ The photoluminescence quantum yield of a sample, Φ_s , can be determined using the equation $\Phi_s = \Phi_r(A_r/A_s)((I_s/I_r)(n_s/n_r)^2)$, where A stands for

the absorbance at the excitation wavelength (λ_{exc} : 360 nm), I is the integrated area under the corrected emission curve and n is the refractive index of the solvent, with the subscripts “s” and “r” representing sample and reference respectively. Poly(methyl methacrylate) (PMMA)-doped (10 wt%) and 1,3-bis(*N*-carbazolyl)benzene (mCP)-doped (10 wt%) thin films were prepared by spin-coating a chlorobenzene solution of the desired sample on a quartz and sapphire substrate. Solid-state Φ_{PL} measurements of thin films were performed in an integrating sphere under a nitrogen atmosphere or air using a Hamamatsu C9920-02 luminescence measurement system. For temperature-dependent measurements, samples prepared on sapphire substrates were cooled down to 77 K in a cryostat (Oxford Instruments). Time-resolved spectra (prompt fluorescence and phosphorescence) were obtained in 10 wt% mCP doped or 10 wt% PMMA doped thin films at 77 K using a gated intensified charge coupled device (iCCD camera) from Stanford Computer Optics and under laser excitation at 360 nm.

Electrochemical measurements: All electrochemical experiments were carried out in 3 mL of DCM with a luminophore and with TBAP as the electrolyte, at concentrations of 0.7 mM and 0.1 M, respectively. A Pt electrode with an active diameter of 2 mm was used as the working electrode and was polished with 1, 0.3 and 0.05 μm aluminum oxide nanoparticles before every use. An electrochemical polish was subsequently performed in 0.1 M H_2SO_4 scanning between -0.9 and 0.9 V vs. Pt wire at a scan rate of 0.5 V/s for 20 minutes. The quality of the polish was verified with cyclic voltammetry of a $[\text{Ru}(\text{bpy})_3]^{2+}$ solution at a scan rate of 0.1 V/s by seeing the 60 mV difference between the cathodic and anodic peaks for the $[\text{Ru}(\text{bpy})_3]^{2+}$ oxidation and the same peak height. Pt coil counter and reference electrodes were used for all measurements, and calibration of the potential was performed with ferrocene as a

reference. All ECL cells were constructed in an inert atmosphere glove box and were sealed to prevent oxygen from entering the cell during experiments.

ECL was measured by a photomultiplier tube (R928 PMT, Hamamtsu Photonics, Japan) held at -750 V. The voltage signal from the PMT was transduced by a Keithley ammeter (6487, Keithley Instruments, Cleveland, OH) into so-called photocurrent measured in nanoamperes (nA).

The spectroscopic measurement methods were reported elsewhere,⁴ with a spectrograph (Acton 2300i, Princeton Instruments Inc., Trenton NJ) coupled with a CCD camera (Model DV420-BV, Andor Technology, UK) cooled to -55 °C.

The relative efficiency of the ECL emission was determined by finding the charge input and the ECL output for the specific experimental setup and comparing these values to the commercial standard of ECL emitter systems, [Ru(bpy)₃]²⁺ for annihilation systems and [Ru(bpy)₃]²⁺/BPO or [Ru(bpy)₃]²⁺/TPrA for co-reactant systems, by the following equation:

$$\Phi_{\text{ECL}} = \frac{\left(\frac{\int \text{ECL dt}}{\int \text{Current dt}} \right)_x}{\left(\frac{\int \text{ECL dt}}{\int \text{Current dt}} \right)_{st}} \times 100 \% \quad (1)$$

where *st* and *x* refer to the standard [Ru(bpy)₃]²⁺ and compounds of interest, respectively. Pulsing annihilation efficiencies were measured from 25 pulses using **Eq. 1**.

Reaction enthalpies were calculated by the following equation:⁵

$$-\Delta H^\circ \leq E^\circ \left(\frac{R^{*+}}{R'} \right) - E^\circ \left(\frac{R}{R^{*-}} \right) - T\Delta S^\circ \quad (2)$$

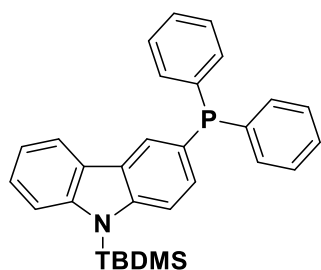
where E° values are the standard reduction potentials for two half reactions and $T\Delta S^\circ$ is equal to 0.1 eV when considering the temperature dependence on half reaction potentials. This measurement has an uncertainty of 0.1 eV.

Theoretical modelling:

The density functional theory (DFT) calculations were performed with the Gaussian 16 revision A.03 suite.⁶ Ground state optimized structures were obtained using PBE0⁷ functional each employing the 6-31G(d,p) basis set with dispersion correction included. Excited state calculations were performed for each within the Tamm-Dancoff approximation (TDA).⁸ The attachment/detachment formalism⁹ was employed to calculate ϕ_s values for each of the excited states using the NANCY package.¹⁰ When mentioned, solvent effects were introduced within the Polarizable Continuum model for the ground state optimization and excited states calculations.¹¹ Molecular orbitals were visualized using GaussView 6.0.16 software.¹²

Synthesis

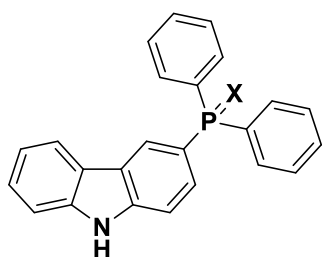
TBDMS-PPCz, (9-(*tert*-butyldimethylsilyl)-3-(diphenylphosphanyl)-9*H*-carbazole)



n-BuLi (1.6 M solution in hexanes, 9 mL, 1.05 equiv.) was added to a solution of 9-TBDMS-3-bromo-9*H*-carbazole (5.00 g, 13.87 mmol, 1.0 equiv.) in dry THF (50 mL) cooled at -78 °C. The reaction mixture was stirred at -78 °C for 30 min.

Chlorodiphenylphosphine (3.672g, 16.64 mmol, 1.2 equiv.) was added and the reaction was allowed to warm up to room temperature and stirred for another 30 min. Water (10 mL) was added to quench the reaction and the organics were extracted with DCM (3×100 mL). The combined organic layer was washed with brine solution and dried over anhydrous sodium sulfate. The crude mixture was purified by column chromatography using 30% DCM/hexanes mixture as the eluent. White solid. **Yield:** 85%. **¹H NMR (400 MHz, CDCl₃) δ:** 8.18 – 8.13 (m, 1H), 8.02 – 7.97 (m, 1H), 7.62 (dd, *J* = 8.4, 7.9 Hz, 2H), 7.44 – 7.32 (m, 12H), 7.27 – 7.21 (m, 1H), 1.08 (d, *J* = 3.0 Hz, 9H), 0.80 – 0.75 (m, 6H). **¹³C{¹H} NMR (101 MHz, CDCl₃) δ:** 145.76, 145.27, 138.10, 138.01, 133.69, 133.50, 131.14, 130.95, 128.50, 128.43, 126.83, 126.40, 126.16, 125.86, 125.61, 119.96, 119.91, 114.44, 114.36, 114.22, 26.59, 20.58, -1.21. **³¹P{¹H} NMR (162 MHz, CDCl₃) δ:** -5.33. GCMS (*m/z*): 466.80 (*R. time*, 15.7 min)

9*H*-carbazol-3-ylidiphenylphosphine oxide/chalcogenide (PPXCz)



X = O, S

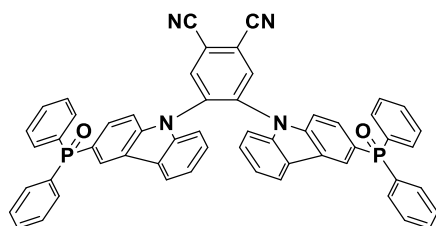
A mixture of **TBDMS-PPCz** (0.50 g, 1.0 mmol, 1 equiv.) and H₂O₂ or S₈ (5.0 equiv.) in THF (10 mL) was stirred at room temperature for 18 h. Tetra-*n*-butylammonium fluoride (1 M solution in THF, 6.2 mL, 6.22 mmol, 3 equiv.) was added and the reaction was stirred for 30 min at room temperature. The reaction mixture was diluted with water and extracted with DCM (2×50 mL). The combined organic layers were dried with anhydrous sodium sulfate and the crude mixture was purified by flash column

chromatography using a gradient of 0-5% MeOH/DCM as the eluent to afford the title compound.

PPOCz: White solid. **Yield:** 95%. **R_f:** 0.5 (5% MeOH/DCM on silica). **Mp:** 308-310 °C. **¹H NMR (400 MHz, DMSO-*d*₆)** δ : 11.71 (s, 1H), 8.47 (d, *J* = 12.3 Hz, 1H), 8.17 (d, *J* = 7.8 Hz, 1H), 7.73 – 7.50 (m, 13H), 7.49 – 7.40 (m, 1H), 7.23 – 7.16 (m, 1H). **¹³C{¹H} NMR (101 MHz, DMSO-*d*₆)** δ : 142.09, 142.06, 140.62, 134.93, 133.91, 132.23, 132.20, 132.08, 131.98, 129.17, 129.06, 128.93, 128.82, 126.93, 124.94, 124.83, 122.94, 122.80, 122.38, 122.05, 121.11, 120.97, 119.91, 111.80, 111.65. **³¹P{¹H} NMR (162 MHz, DMSO-*d*₆)** δ : 26.82. **HR-MS (ESI) [M+H]⁺ Calculated:** 368.1199; **Found:** 368.1208.

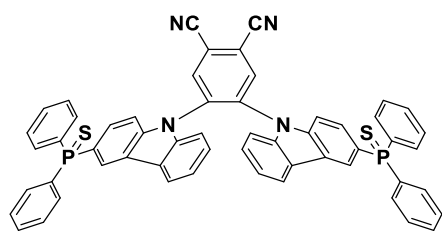
PPSCz: White solid. **Yield:** 95 %. **R_f:** 0.5 (5% MeOH/DCM on silica). **Mp:** 228-230 °C. **¹H NMR (400 MHz, CDCl₃)** δ : 11.94 (s, 1H), 8.47 (dd, *J* = 14.3, 1.4 Hz, 1H), 7.94 (d, *J* = 7.8 Hz, 1H), 7.86 (dd, *J* = 8.5, 2.3 Hz, 1H), 7.78 – 7.69 (m, 5H), 7.55 – 7.46 (m, 3H), 7.46 – 7.38 (m, 4H), 7.33 – 7.26 (m, 2H), 7.16 – 7.09 (m, 1H). **¹³C{¹H} NMR (101 MHz, CDCl₃)** δ : 142.35, 140.98, 134.54, 133.70, 132.33, 132.23, 131.25, 128.44, 128.31, 126.05, 125.21, 125.08, 122.37, 120.06, 119.14, 112.43, 112.20. **³¹P{¹H} NMR (162 MHz, CDCl₃)** δ 44.41. **HR-MS (ESI) [M+H]⁺ Calculated:** 384.0976; **Found:** 384.0979.

PPOCzPN(4,5-bis(3-(diphenylphosphoryl)-9*H*-carbazol-9-yl)phthalonitrile):



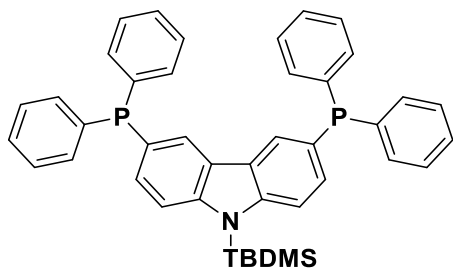
To a solution of **PPOCz** (250 mg, 0.68 mmol, 2 equiv.) in dry THF (5 mL) was added sodium hydride (60% in mineral oil, 40.8 mg, 1.02 mmol, 3 equiv.) and the mixture was stirred for 30 mins. 4,5-difluorophthalonitrile (55.8 mg, 0.34 mmol, 1 equiv.) was added and the reaction mixture was stirred for further 6 h. Water (5 mL) was added and the organics were extracted with DCM (3 × 10 mL). The combined organics were dried with anhydrous magnesium sulfate and the crude was purified by flash column chromatography using 0-5% MeOH/DCM as the eluent to afford the title compound. Pale yellow solid. **Yield:** 96%. **R_f:** 0.5 (5 % MeOH/DCM on silica). **Mp:** 220-221 °C. **¹H NMR (400 MHz, CDCl₃) δ:** 8.38 (s, 1H, **PPOCzPN-2**), 8.37 (s, 1H, **PPOCzPN-1**), 8.23 (d, *J* = 12.2 Hz, 1H, **PPOCzPN-1**), 8.13 (d, *J* = 12.1 Hz, 1H, **PPOCzPN-2**), 7.76 (d, *J* = 7.5 Hz, 1H, **PPOCzPN-1**), 7.66 (d, *J* = 7.7 Hz, 1H, **PPOCzPN-2**), 7.61 – 7.40 (m, 21H), 7.25 – 6.92 (m, 7H), 6.75 (dd, *J* = 8.5, 1.7 Hz, 1H). **¹³C{¹H} NMR (101 MHz, CDCl₃) δ:** 139.98, 139.66, 138.75, 138.54, 137.73, 137.56, 135.54, 135.50, 133.29, 133.16, 133.02, 132.25, 131.99, 131.89, 129.56, 129.44, 129.09, 128.97, 128.65, 128.60, 128.53, 128.48, 127.48, 127.19, 125.74, 125.48, 125.14, 125.04, 124.70, 124.60, 124.41, 124.36, 124.22, 123.95, 123.82, 123.65, 123.52, 122.73, 122.63, 120.88, 120.81, 115.81, 115.64, 114.15, 109.48, 109.34, 109.10, 109.02, 108.88, 108.75. **³¹P{¹H} NMR (162 MHz, CDCl₃) δ:** 29.62 (**PPOCzPN-2**), 29.51 (**PPOCzPN-1**). **HR-MS (ESI) [M+H]⁺ Calculated:** 859.2313; **Found:** 859.2375. **Elemental analysis (C₅₆H₃₆N₄O₂P₂) calculated:** C, 78.31; H, 4.23; N, 6.52; **Found:** C, 77.56; H, 4.28; N, 6.46.

PPSCzPN (4,5-bis(3-(diphenylphosphorothioyl)-9*H*-carbazol-9-yl)phthalonitrile):



The title compound was prepared in the same way as **PPOCzPN**, except **PPSCz** was used as the starting material. Yellow solid. **Yield:** 90 %. **R_f:** 0.5 (5 % MeOH/DCM on silica). **Mp:** 196-197 °C. **¹H NMR (400 MHz, DMSO-*d*₆)** δ: 9.02 (d, *J* = 3.0 Hz, 2H), 8.24 (d, *J* = 13.6 Hz, 2H, **PPSCzPN-2**), 7.89 (dd, *J* = 27.7, 7.3 Hz, 2H, **PPSCzPN-1**), 7.48 (td, *J* = 30.2, 9.7 Hz, 21H), 7.35 – 6.94 (m, 7H), 6.94 – 6.74 (m, 1H). **¹³C{¹H} NMR (101 MHz, DMSO-*d*₆)** δ: 140.44, 140.11, 139.55, 139.29, 137.67, 137.42, 137.10, 137.02, 134.07, 133.95, 133.70, 133.22, 133.10, 132.86, 132.19, 132.04, 131.97, 131.95, 131.87, 129.43, 129.25, 129.13, 128.74, 128.62, 127.42, 127.22, 124.65, 124.52, 124.39, 124.26, 124.20, 123.63, 123.53, 123.49, 123.38, 123.32, 122.80, 122.31, 120.92, 116.32, 116.16, 115.74, 110.75, 110.58. **³¹P{¹H} NMR (162 MHz, DMSO-*d*₆)** δ: 42.87. **HR-MS (ESI) [M+H]⁺ Calculated:** 891.1929; **Found:** 891.1918. **Elemental analysis (C₅₆H₃₆N₄S₂P₂) calculated:** C, 75.49; H, 4.07; N, 6.29. **Found:** C, 75.38; H, 3.98; N, 6.30.

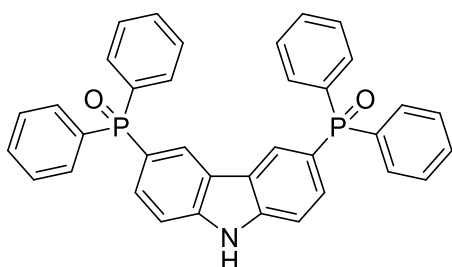
TBDMS-DiPPCz (9-(*tert*-butyldimethylsilyl)-3,6-bis(diphenylphosphanyl)-9H-carbazole)



The title compound was prepared in a similar manner as **TBDMS-PPCz**, except 9-TBDMS-3,6-dibromo-9H-carbazole was used as starting material. **Yield:** 60%. **¹H**

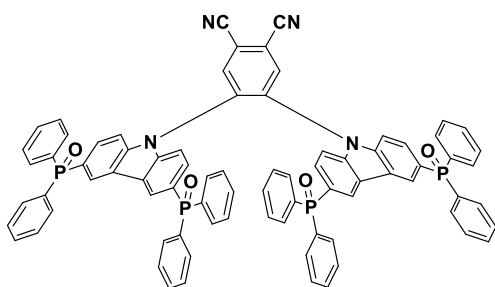
NMR (400 MHz, CDCl₃) δ : 8.08 (dd, J = 8.5, 1.2 Hz, 1H), 7.65 (d, J = 8.6 Hz, 1H), 7.52 – 7.31 (m, 8H), 1.12 (d, J = 5.3 Hz, 3H), 0.83 – 0.78 (m, 2H). **¹³C{¹H} NMR (101 MHz, CDCl₃)** δ : 145.93, 138.17, 138.07, 133.70, 133.51, 131.48, 131.29, 128.54, 128.47, 126.84, 126.76, 126.52, 126.45, 126.36, 126.27, 114.57, 114.50, 34.75, 31.67, 27.00, 26.61, 25.37, 22.78, 22.74, 20.56, 14.22, -1.20. **³¹P{¹H} NMR (162 MHz, CDCl₃)** δ : -5.48. **HR-MS (ESI) [M+H]⁺ calculated:** 650.2562.

DiPPOCz (3,6-bis(diphenylphosphine oxide)-9H-carbazole)



The title compound was prepared in a similar manner as **PPOCz**. White solid. **Yield:** 95 %. **R_f:** 0.5 (5 % MeOH/DCM on silica). **Mp:** 311-313 °C. **¹H NMR (400 MHz, DMSO-*d*₆)** δ : 12.09 (s, 1H), 8.54 (d, J = 12.2 Hz, 2H), 7.75 – 7.49 (m, 24H). **¹³C{¹H} NMR (101 MHz, DMSO)** δ : 142.54, 134.73, 133.71, 132.25, 132.08, 131.98, 129.75, 129.63, 129.17, 129.06, 125.54, 125.43, 123.23, 122.54, 122.40, 122.15, 112.27, 112.14. **³¹P{¹H} NMR (162 MHz, DMSO)** δ : 26.56. **HR-MS (ESI) [M+H]⁺ Calculated:** 568.1517; **Found:** 568.1576.

DiPPOCzPN (4,5-bis(3,6-bis(diphenylphosphoryl)-9H-carbazol-9-yl)phthalonitrile)



The title compound was prepared in a similar manner as **PPOCzPN**, except **DIPPOCz** was used as the starting material. White-grey solid. **Yield:** 52 %. **R_f:** 0.5 (5 % MeOH/DCM on silica). **Mp:** 280-282 °C. **¹H NMR (400 MHz, CDCl₃) δ:** 8.39 (s, 2H), 8.10 – 8.00 (m, 4H), 7.59 – 7.50 (m, 8H), 7.49 – 7.39 (m, 32H), 7.36 (ddd, *J* = 10.8, 8.6, 1.2 Hz, 4H), 7.10 – 7.05 (m, 4H). **¹³C{¹H} NMR (101 MHz, CDCl₃) δ:** 140.39, 136.93, 135.49, 132.49, 132.42, 132.33, 131.87, 131.80, 131.77, 131.71, 131.44, 131.38, 130.49, 130.38, 128.82, 128.79, 128.70, 128.67, 127.18, 126.13, 125.17, 125.06, 123.46, 123.32, 116.67, 113.78, 109.50, 109.37. **³¹P{¹H} NMR (162 MHz, CDCl₃) δ:** 29.31. **HR-MS (ESI) [M+H]⁺ Calculated:** (C₈₀H₅₄N₄O₄P₄) 1259.3096; **Found:** 1259.3139. **Elemental Analysis (calculated):** C, 76.31; H, 4.32; N, 4.45; **Found:** C, 76.46; H, 4.34; N, 4.59.

Spectra

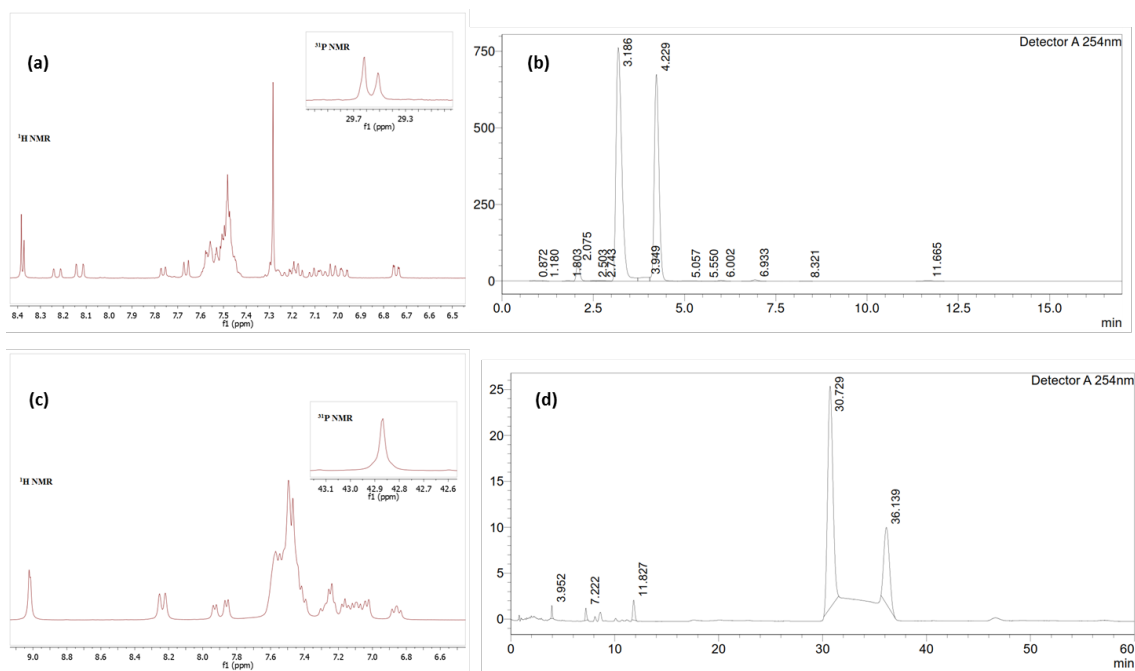


Figure S1. (a) ^1H NMR (inset: ^{31}P NMR) and (b) HPLC trace of **PPOCzPN**. (c) ^1H NMR (inset: ^{31}P NMR) and (d) HPLC trace of **PPSCzPN**.

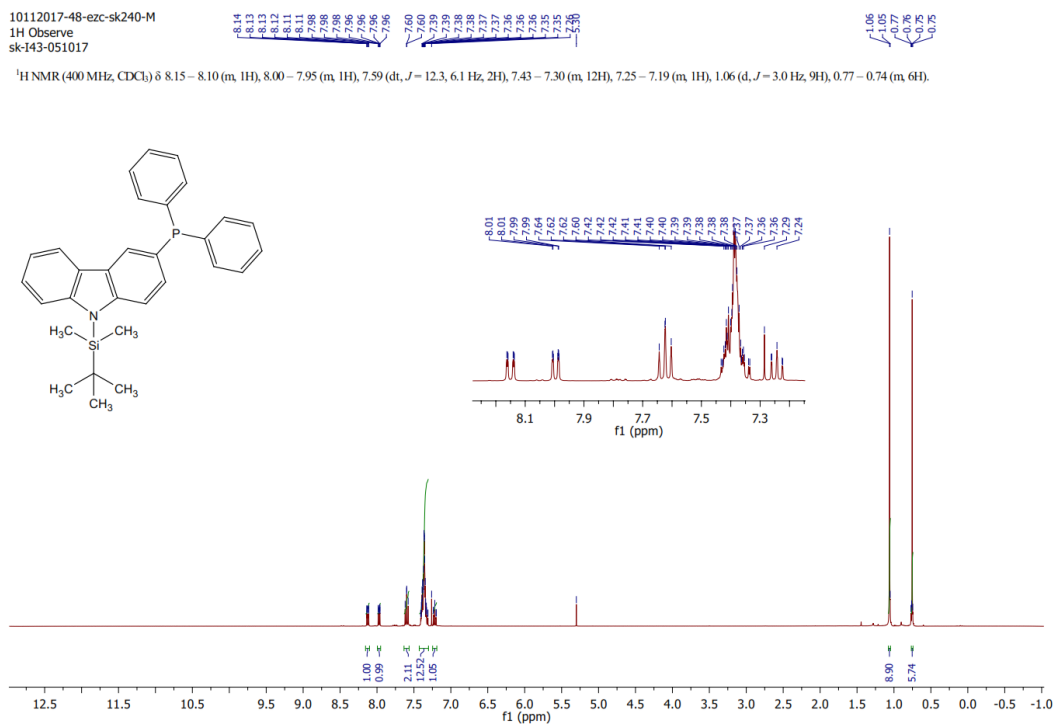


Figure S2. ¹H NMR of TBDMS-PPCz in CDCl₃.

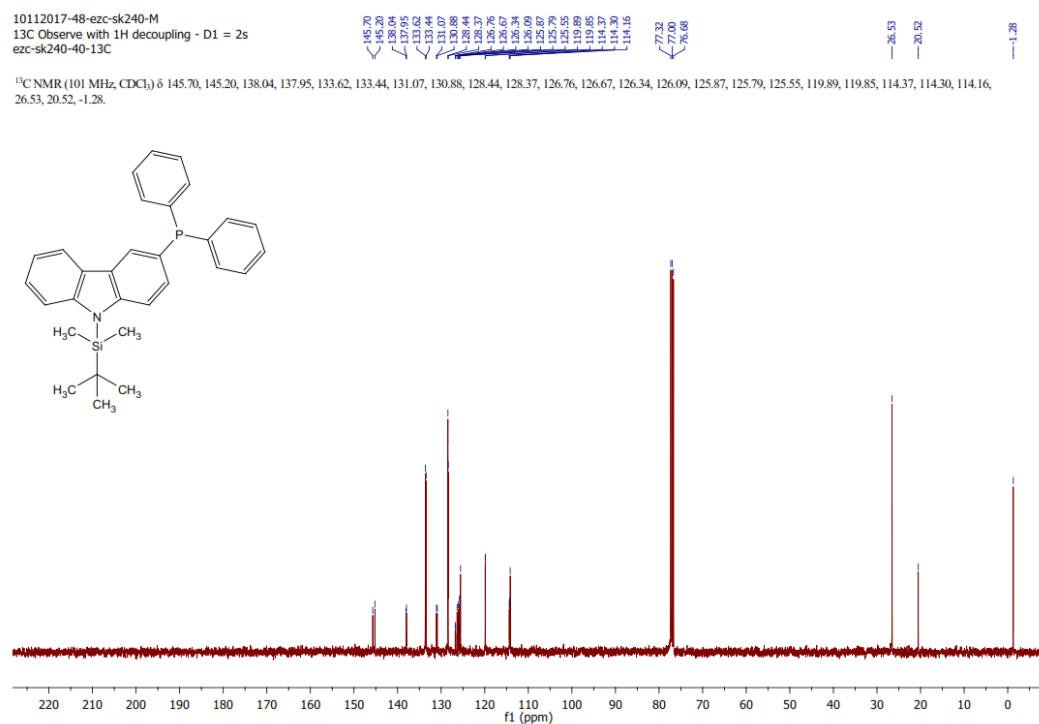


Figure S3. ¹³C{¹H} NMR of TBDMS-PPCz in CDCl₃.

10112017-48-ezc-sk240-M
31P Observe with 1H decoupling
ezc-sk240-40-31P

^{31}P NMR (162 MHz, CDCl_3) δ -5.33.

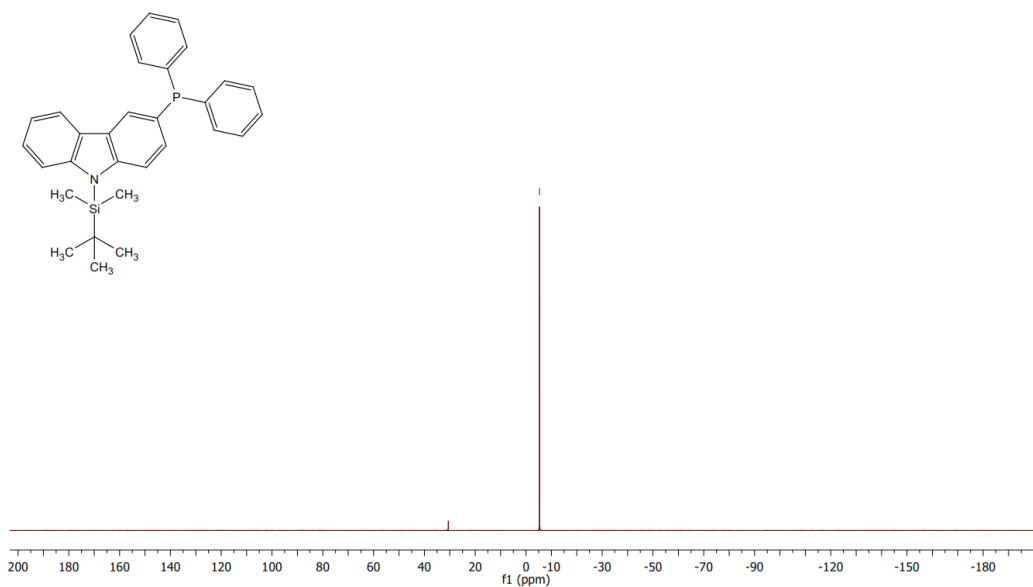


Figure S4. $^{31}\text{P}\{^1\text{H}\}$ NMR of TBDMS-PPCz in CDCl_3 .

11212017-19-ezc-sk240-N
1H Observe
sk-162

^1H NMR (400 MHz, DMSO) δ 11.71 (s, 1H), 8.59 – 8.35 (m, 1H), 8.27 – 8.06 (m, 1H), 7.77 – 7.48 (m, 12H), 7.48 – 7.35 (m, 1H), 7.29 – 7.07 (m, 1H).

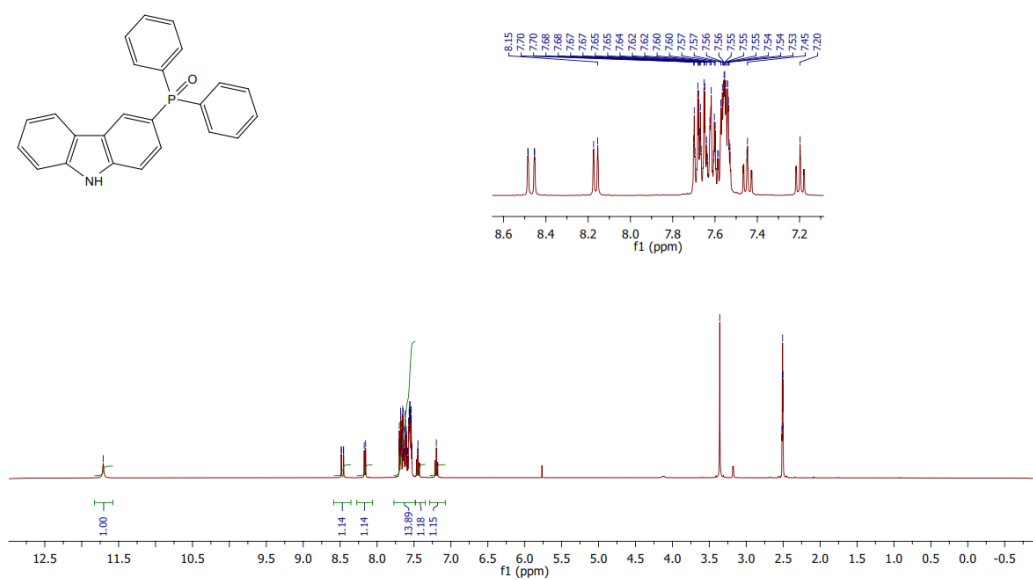


Figure S5. ^1H NMR of PPOCz in DMSO.

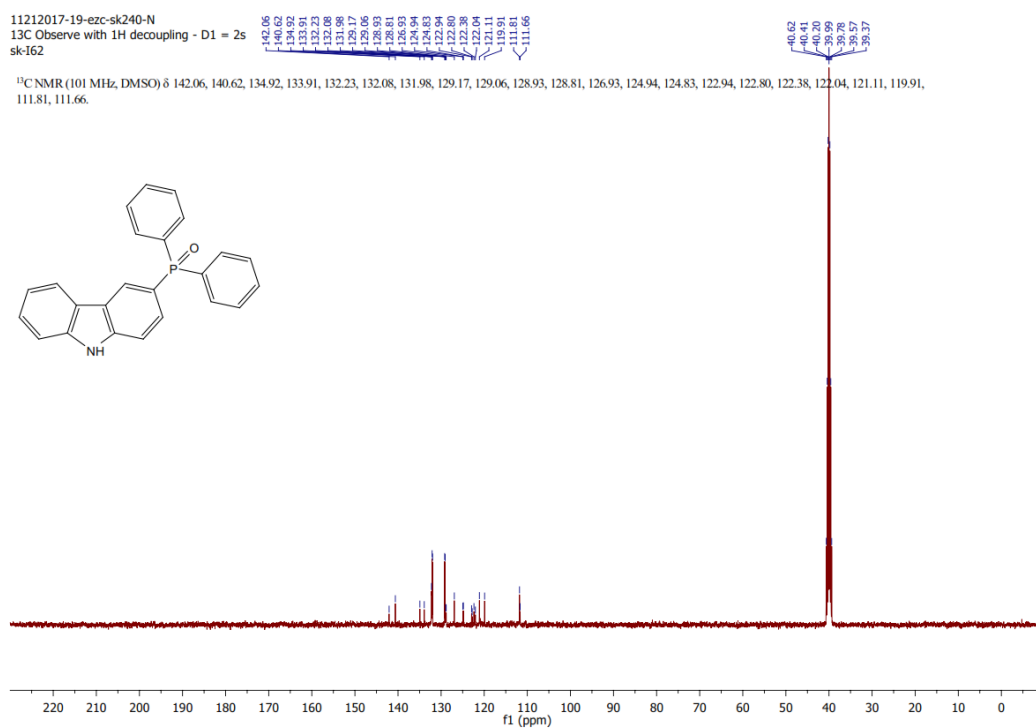


Figure S6. ¹³C{¹H} NMR of PPOCz in DMSO.

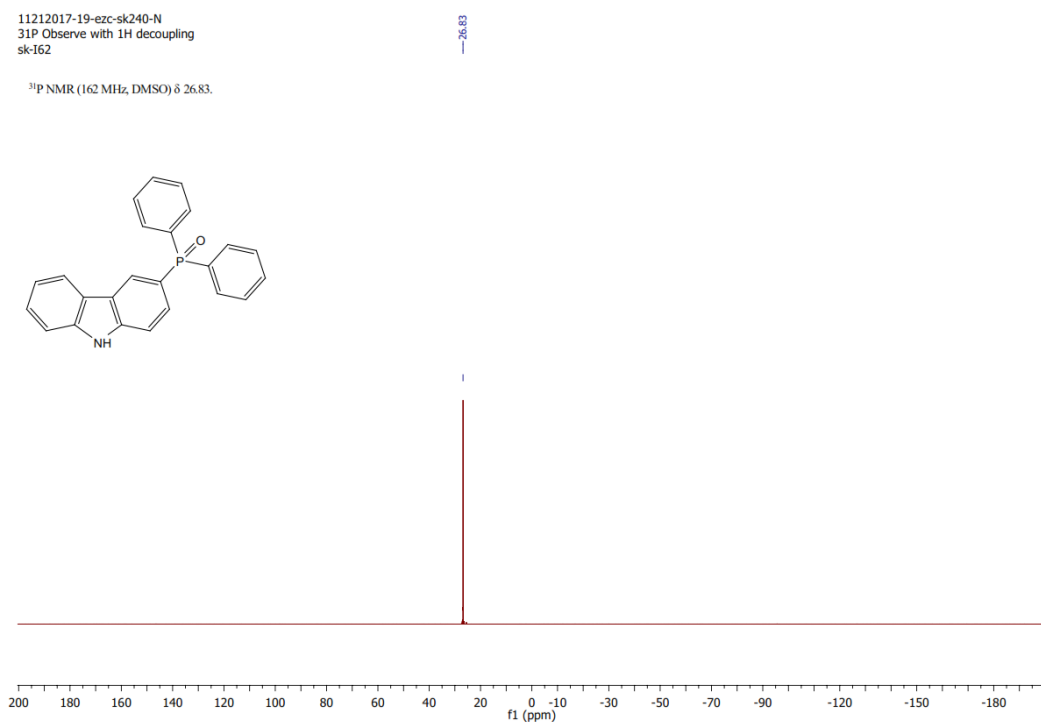


Figure S7. ³¹P{¹H} NMR of PPOCz in DMSO.

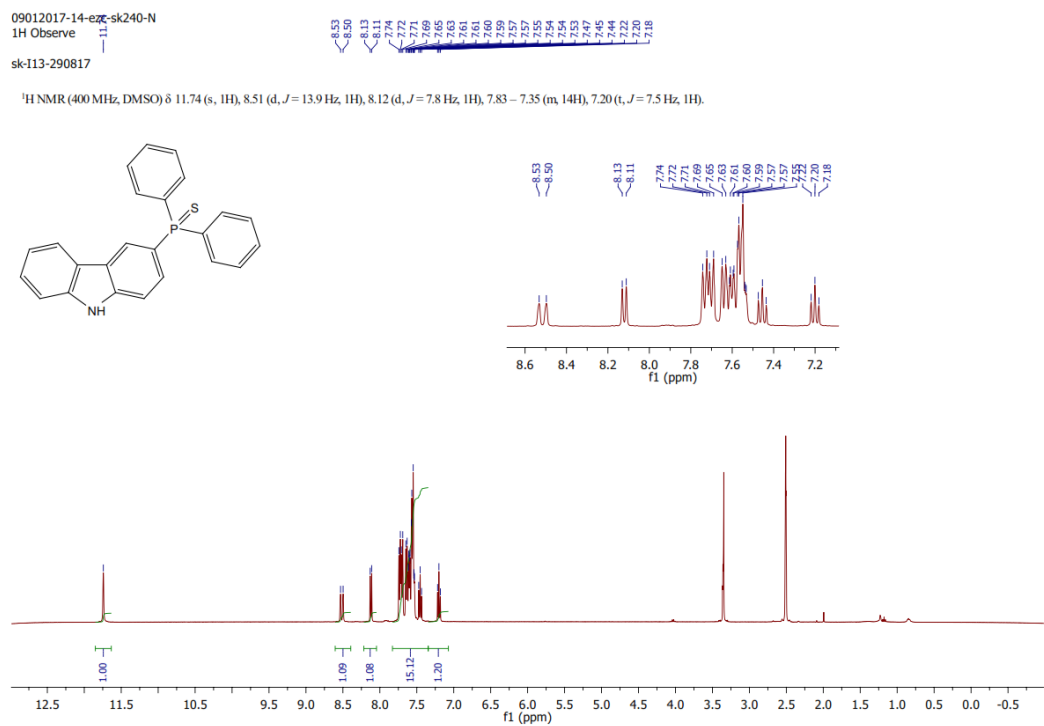


Figure S8 . ¹H NMR of PPSCz in DMSO.

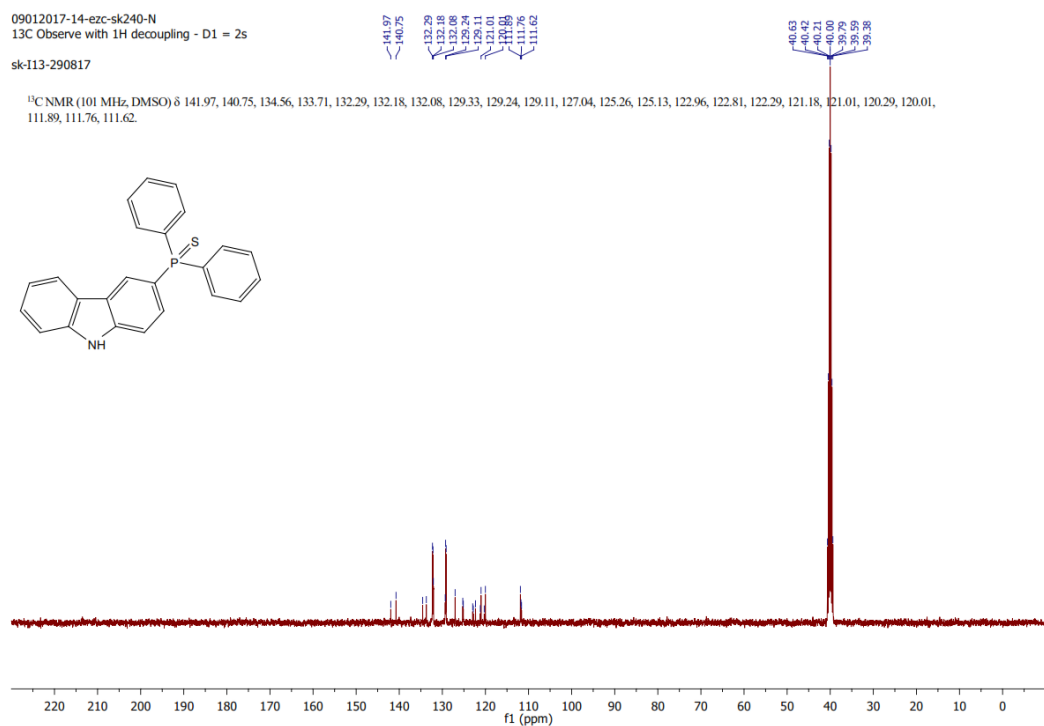


Figure S9. ¹³C{¹H} NMR of PPSCz in DMSO.

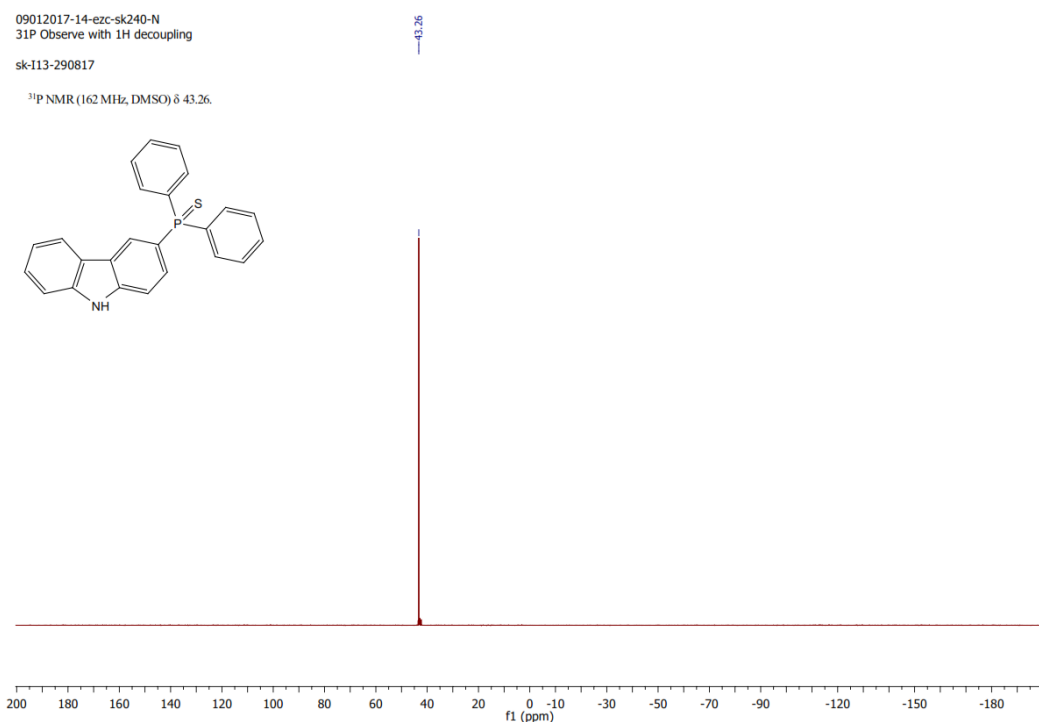


Figure S10. $^{31}\text{P}\{^1\text{H}\}$ NMR of PPSCz in DMSO.

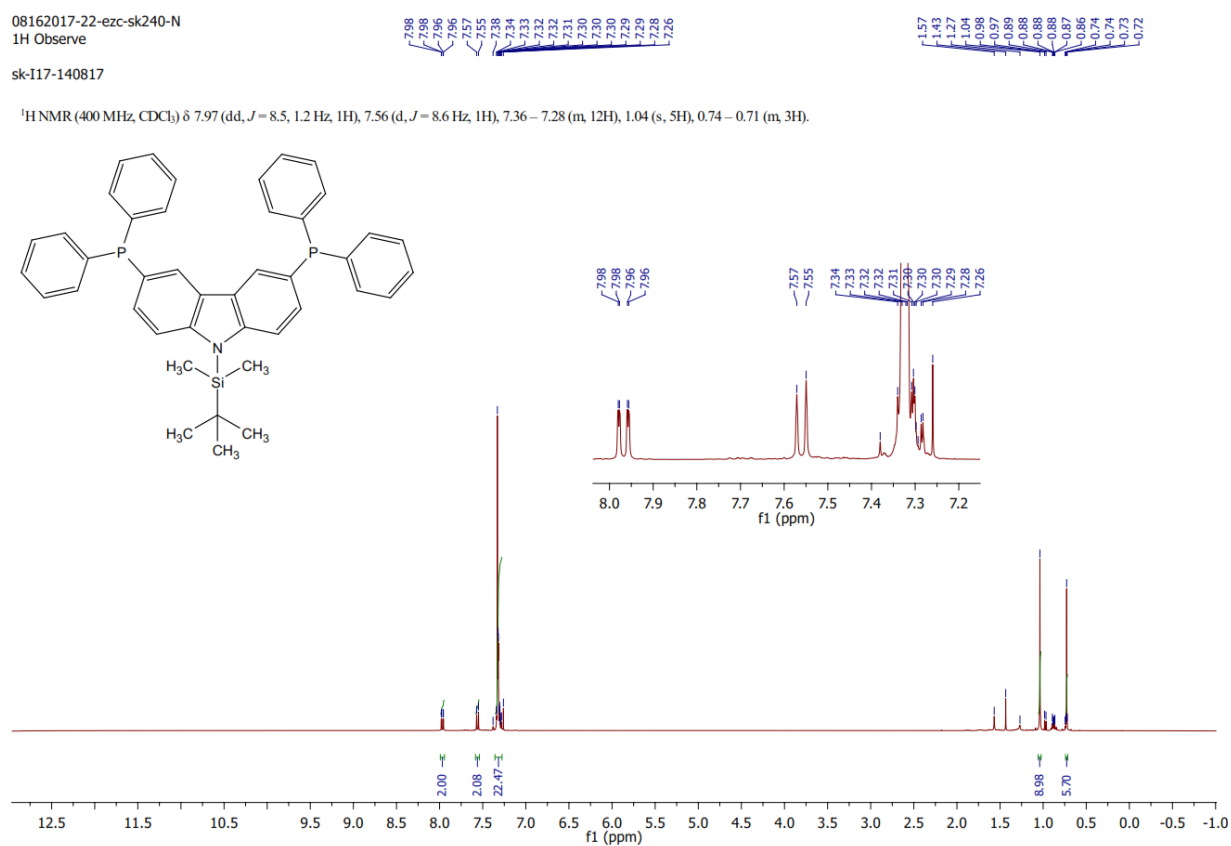


Figure S11. ^1H NMR of TBDMS-DiPPCz in CDCl_3 .



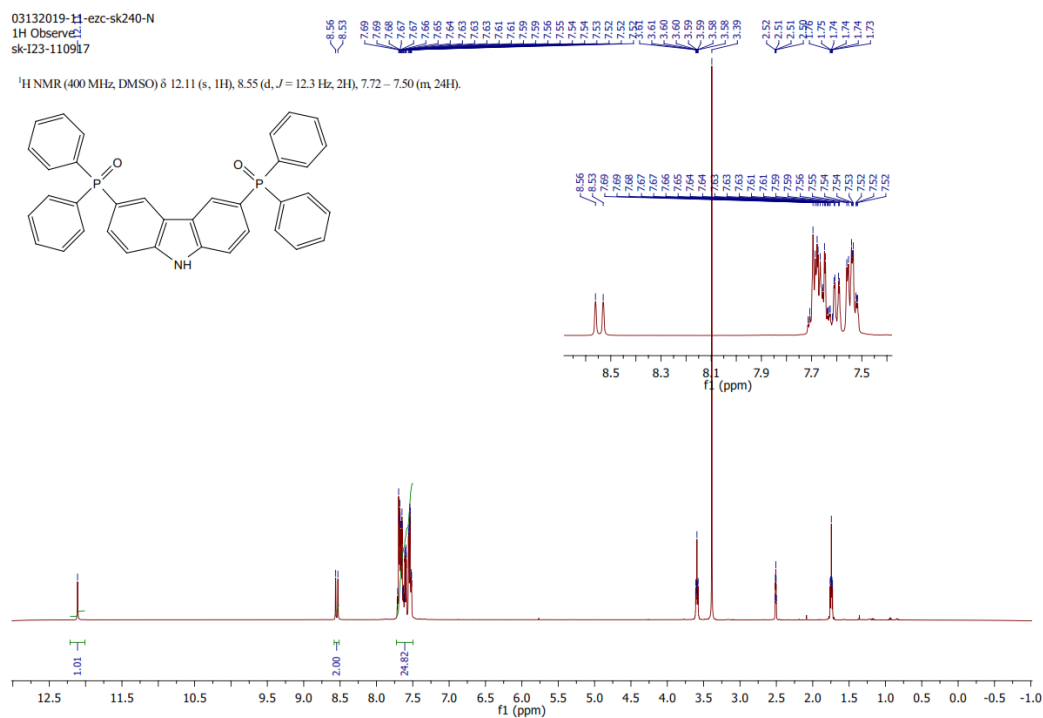


Figure S14. ¹H NMR of DiPPOCz in DMSO.

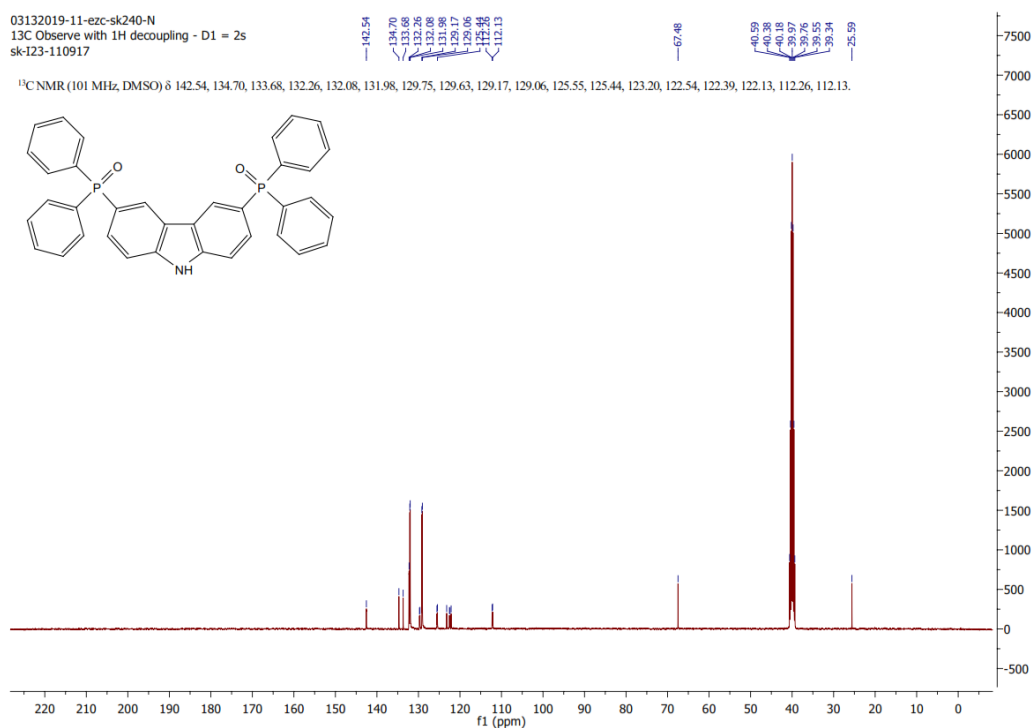


Figure S15. ¹³C{¹H} NMR of DiPPOCz in DMSO.

03132019-11-ezc-sk240-N
 31P Observe with 1H decoupling
 sk-123-110917

^{31}P NMR (162 MHz, DMSO) δ 26.60.

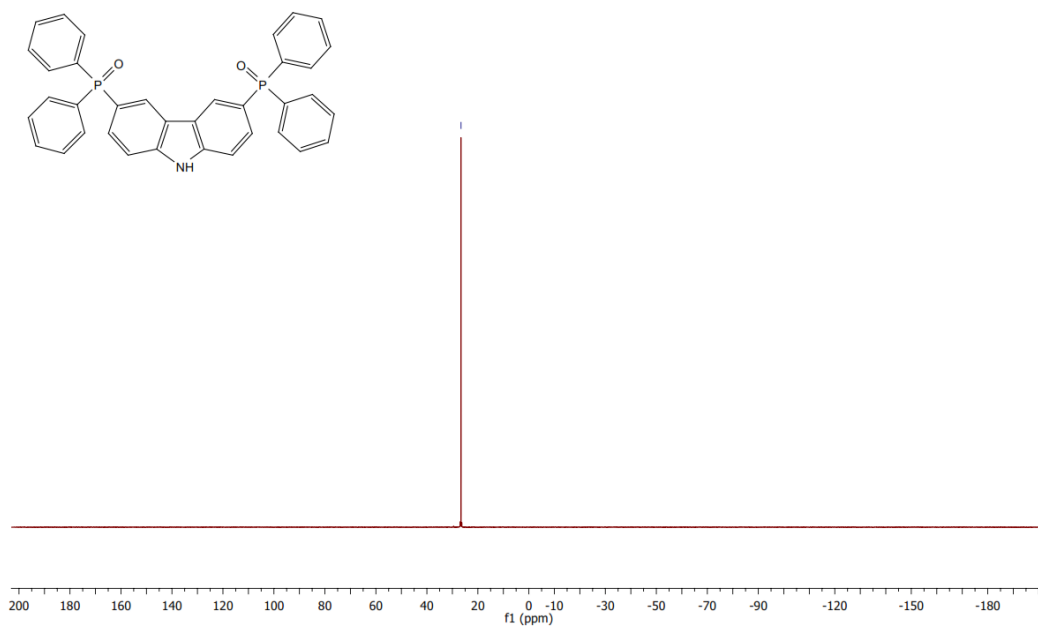


Figure S16. $^{31}\text{P}\{^1\text{H}\}$ NMR of DiPPOCz in DMSO.

01262018-14-ezc-sk240-N
 1H Observe
 sk-172-230118

^1H NMR (400 MHz, Chloroform- d) δ 8.38 (d, J = 4.8 Hz, 2H), 8.23 (d, J = 12.2 Hz, 1H), 8.13 (d, J = 12.1 Hz, 1H), 7.76 (d, J = 7.5 Hz, 1H), 7.66 (d, J = 7.7 Hz, 1H), 7.61 – 7.40 (m, 21H), 7.25 – 6.92 (m, 7H), 6.75 (dd, J = 8.5, 1.7 Hz, 1H).

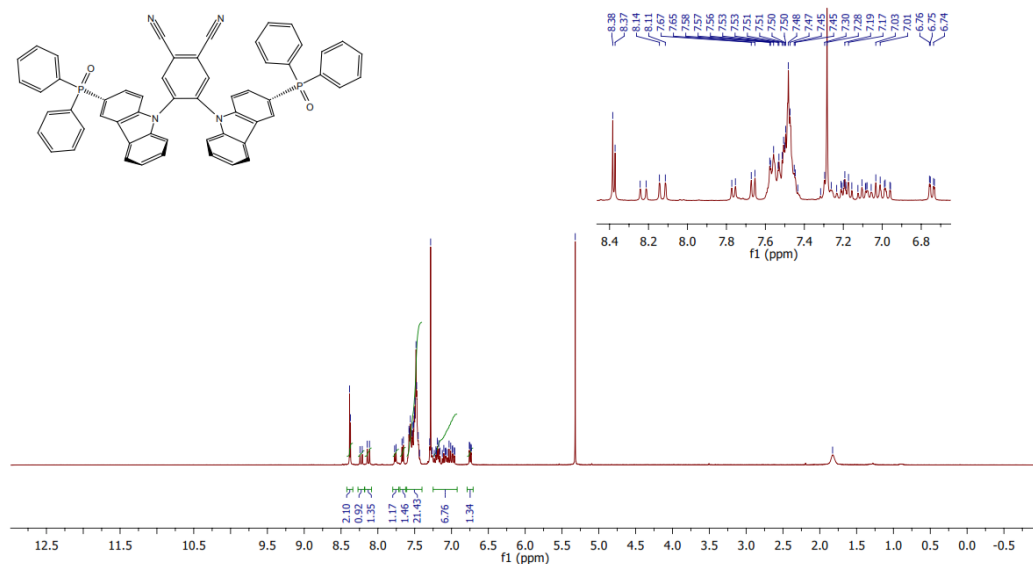


Figure S17. ^1H NMR of PPOCzPN in CDCl_3 .

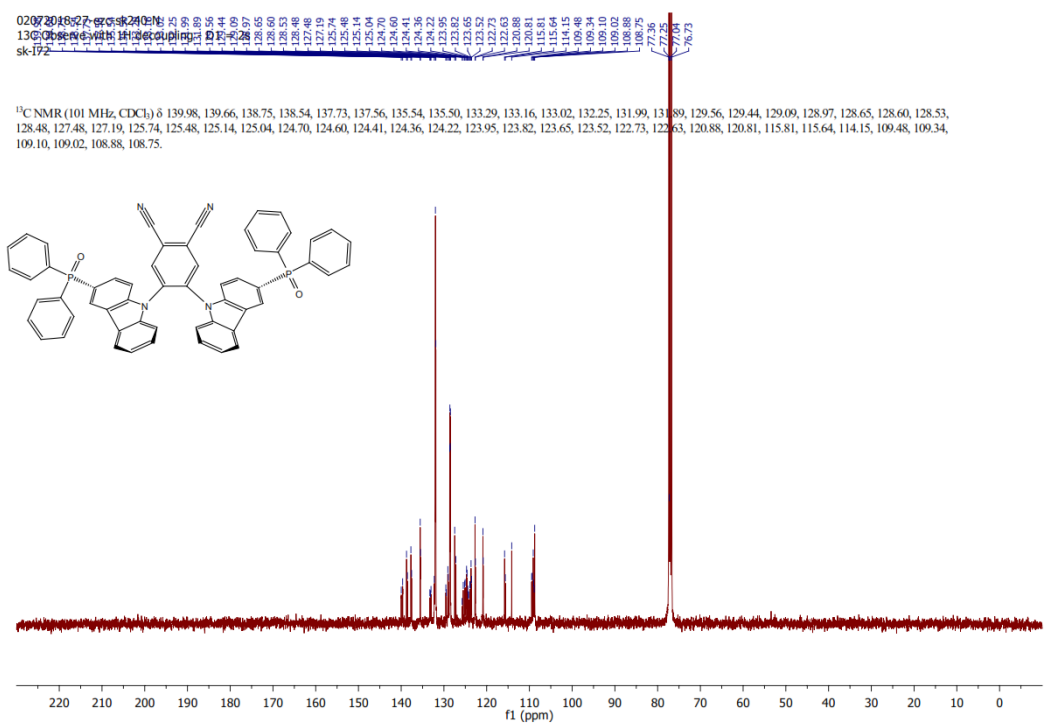


Figure S18. $^{13}\text{C}\{^1\text{H}\}$ NMR of PPOCzPN in CDCl_3 .

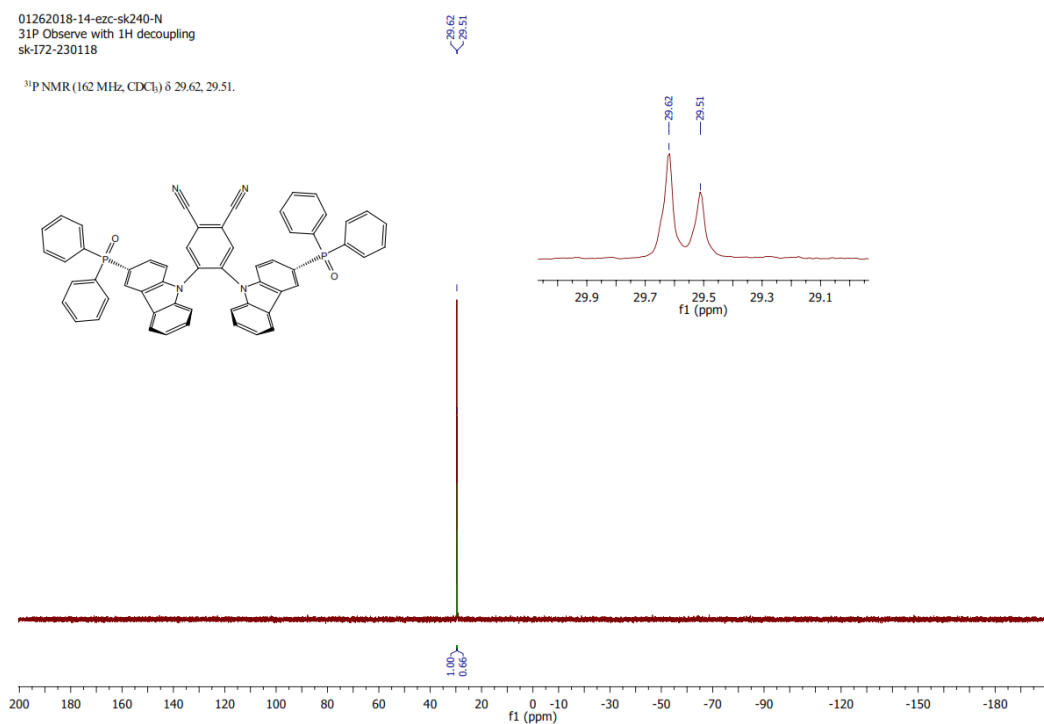


Figure S19. $^{31}\text{P}\{^1\text{H}\}$ NMR of PPOCzPN in CDCl_3 .

PPOCzPN
(DCM)/MeOH + NH₄OAc
C₅₆H₃₆N₄O₂P₂

EPSRC National Facility Swansea
LTQ Orbitrap XL

STAZYS-sk240
19/02/2018 15:19:14

STAZYS_KWTHR_41939 #104-112 RT: 1.51-1.74 AV: 9 SM: 7G NL: 1.32E7
T: FTMS + p NSI Full ms [300.00-4000.00]

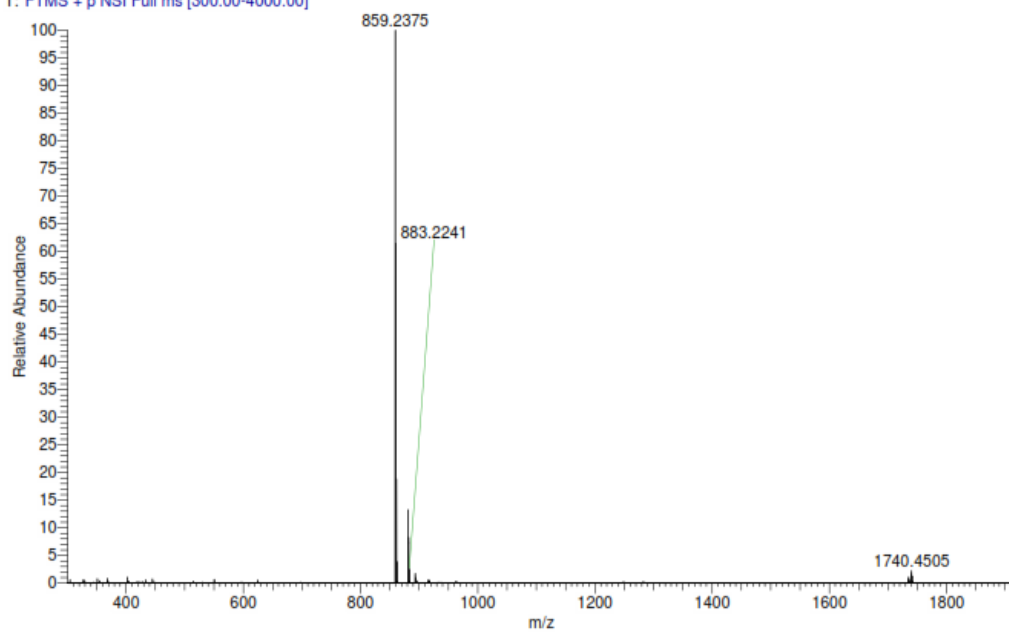


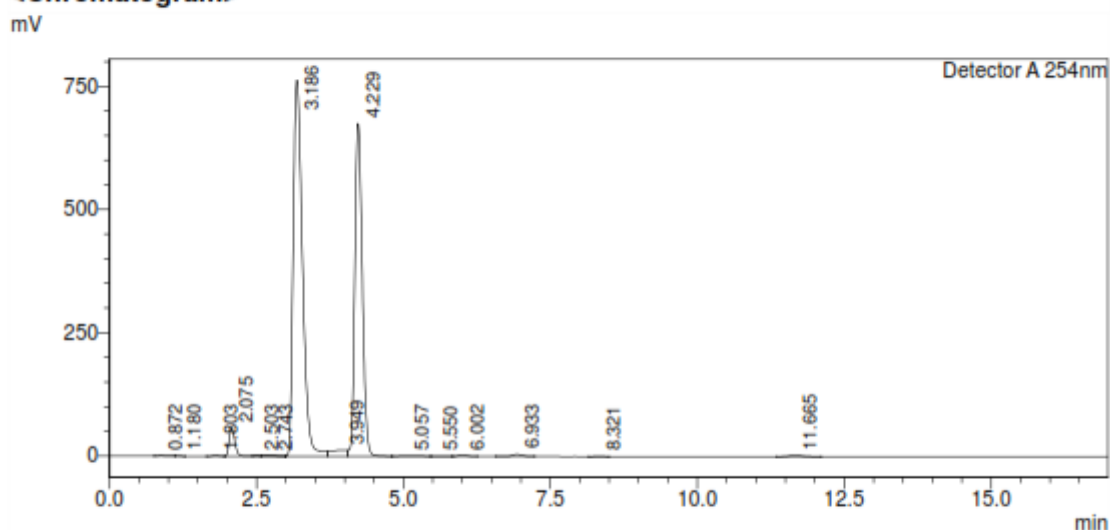
Figure S20. HRMS of PPOCzPN.

HPLC Trace Report12Apr2018

<Sample Information>

Sample Name	: sk-I72	Sample Type	: Unknown
Sample ID	: sk-I72		
Method Filename	: AcN (65).lcm		
Batch Filename	:		
Vial #	: 1-72		
Injection Volume	: 5 uL		
Date Acquired	: 29/03/2018 11:09:08	Acquired by	: ezc-7
Date Processed	: 29/03/2018 17:05:06	Processed by	: ezc-7

<Chromatogram>



<Peak Table>

Detector A 254nm

Peak#	Ret. Time	Area	Height	Area%	Area/Height	Width at 5% Height
1	0.872	4782	615	0.032	7.776	0.308
2	1.180	1012	235	0.007	4.301	0.136
3	1.803	11426	1473	0.076	7.757	--
4	2.075	391371	57074	2.593	6.857	0.216
5	2.503	3249	659	0.022	4.930	--
6	2.743	16676	1357	0.110	12.286	--
7	3.186	8369380	762985	55.448	10.969	0.358
8	3.949	234557	12515	1.554	18.742	--
9	4.229	5948852	675045	39.412	8.813	0.285
10	5.057	14049	727	0.093	19.333	--
11	5.550	2060	155	0.014	13.315	--
12	6.002	20495	2187	0.136	9.371	0.301
13	6.933	44222	4155	0.293	10.642	0.349
14	8.321	1092	113	0.007	9.636	0.285
15	11.665	30787	2209	0.204	13.937	0.462
Total		15094011	1521505	100.000		

Figure S21. HPLC trace analysis of **PPOCzPN**.

Elemental Analysis Service Request Form

Researcher name Dongyang Chen

Researcher email dc217@st-andrews.ac.uk

NOTE: Please submit ca. 10 mg of sample

Sample reference number	dc-III 13
Name of Compound	PPOCzPN
Molecular formula	C ₅₆ H ₃₆ N ₄ O ₂ P ₂
Stability	stable
Hazards	low hazard
Other Remarks	

Analysis type:

Single ☐ Duplicate ☒ Triplicate ☐

Analysis Result:

Element	Expected %	Found (1)	Found (2)	Found (3)
Carbon	78.31	77.43	77.56	
Hydrogen	4.23	4.24	4.28	
Nitrogen	6.52	6.47	6.46	
Oxygen				

Authorising Signature:

Date completed	21.05.21
Signature	J-PC
comments	

Figure S22. Elemental analysis report for PPOCzPN.

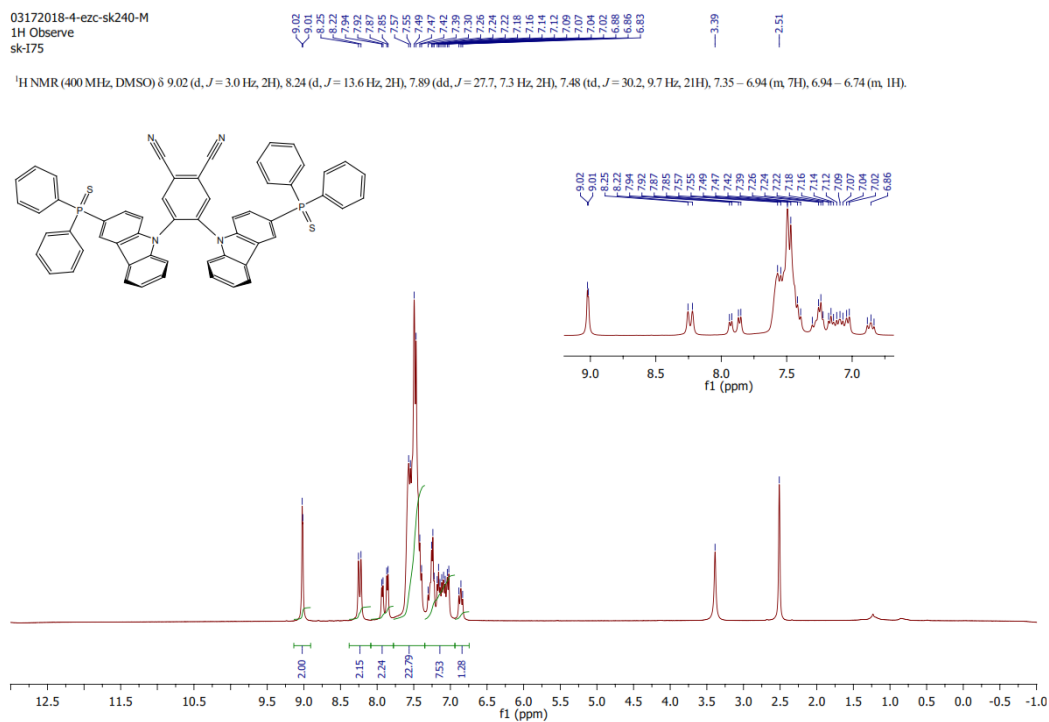


Figure S23. ¹H NMR of PPSCzPN in CDCl₃.

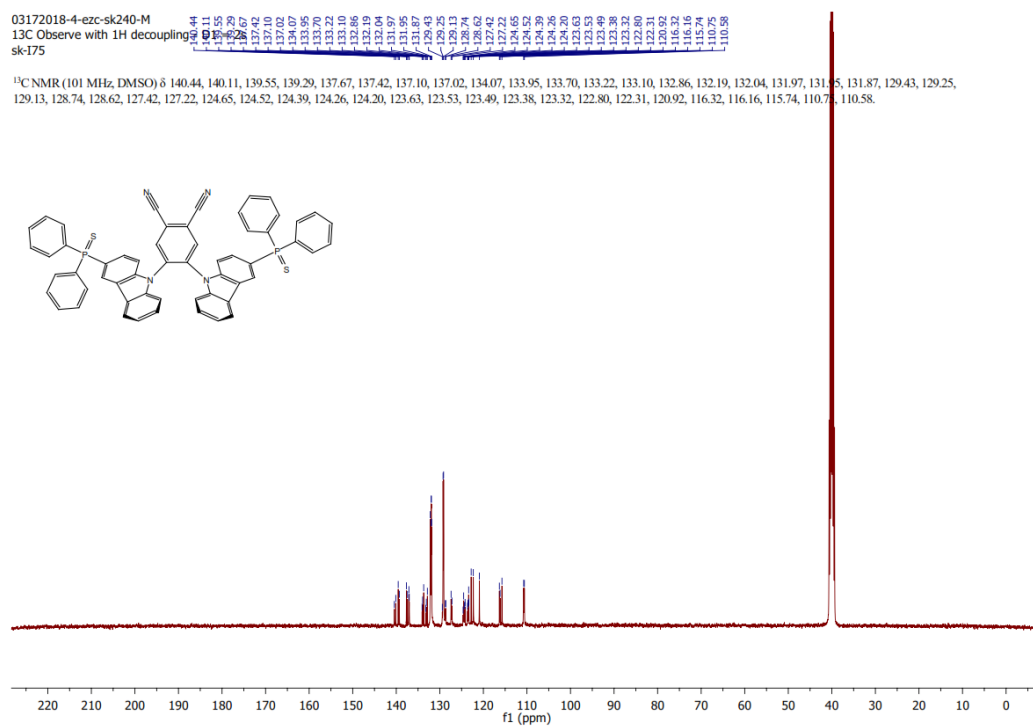


Figure S24. ¹³C{¹H} NMR of PPSCzPN in CDCl₃.

03172018-4-ezc-sk240-M
31P Observe with 1H decoupling
sk-175

^{31}P NMR (162 MHz, DMSO) δ 42.87.

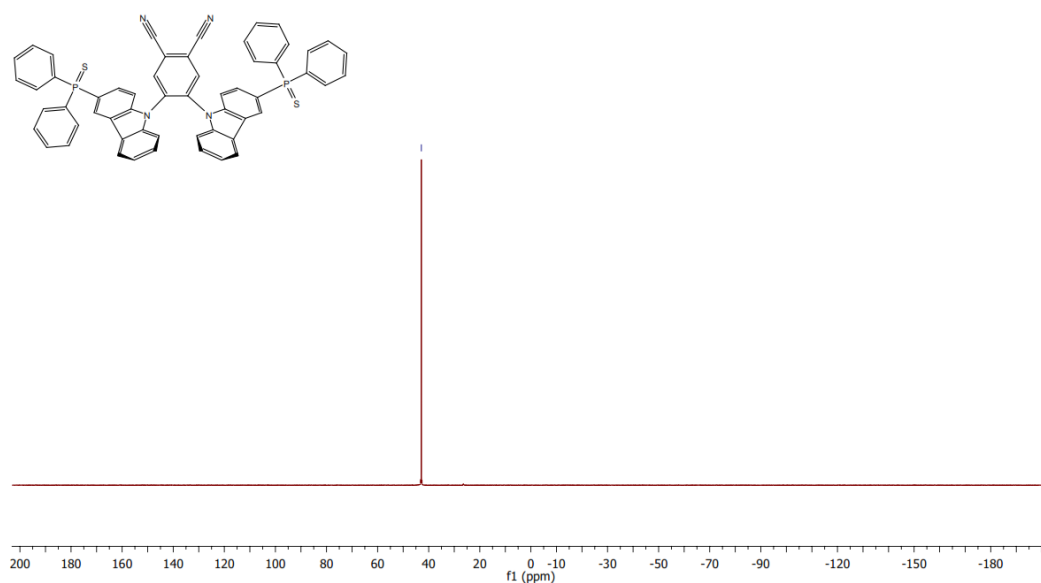


Figure S25. $^{31}\text{P}\{^1\text{H}\}$ NMR of PPSCzPN in CDCl_3 .

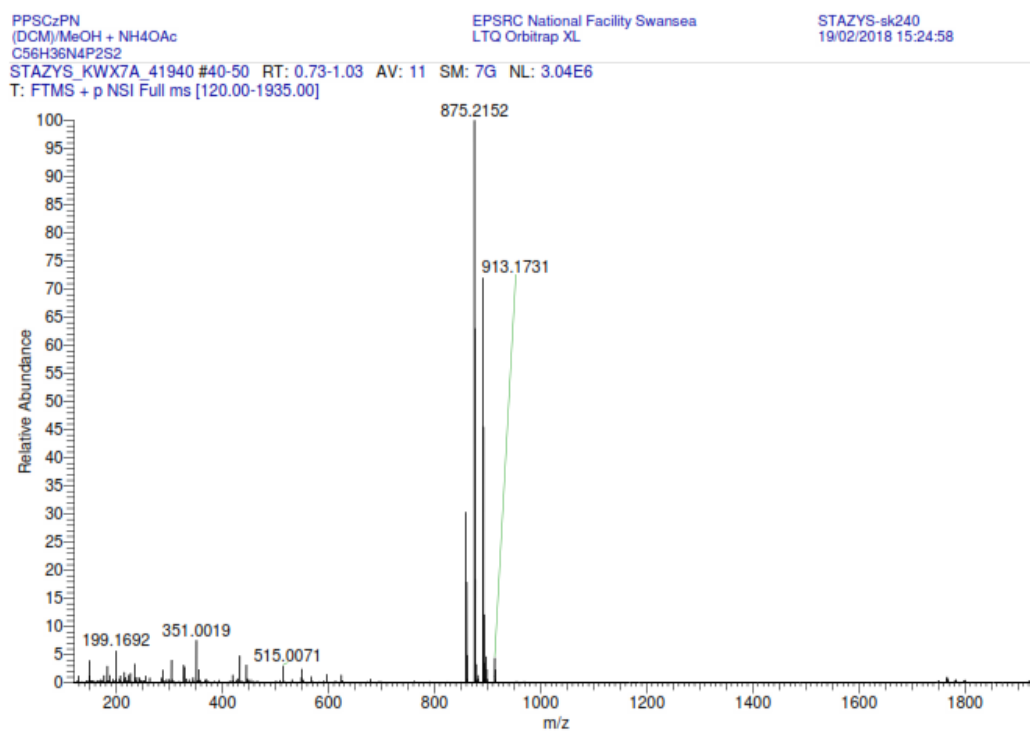


Figure S26. HRMS of PPSCzPN.

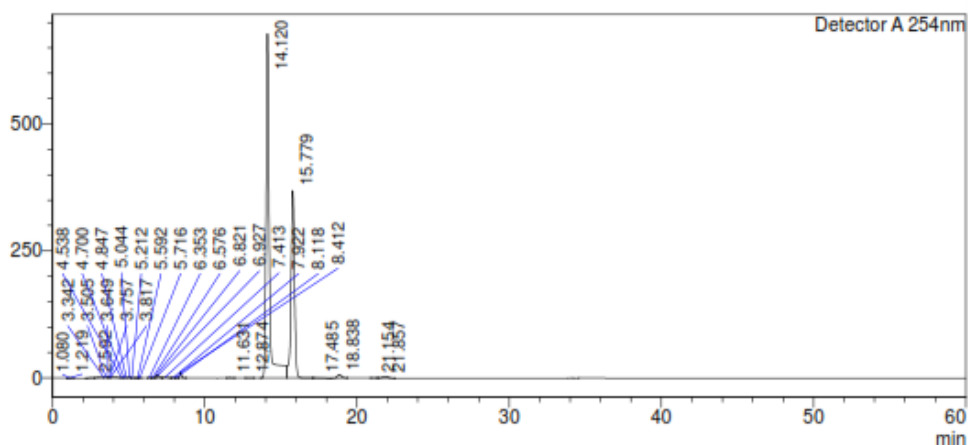
HPLC Trace Report12Apr2018

<Sample Information>

Sample Name : SK-I75
 Sample ID : SK-I75
 Method Filename : AcN (75).lcm
 Batch Filename : 2ndGenTADF_2.lcb
 Vial # : 1-75
 Injection Volume : 5 uL
 Date Acquired : 29/03/2018 17:44:17
 Date Processed : 29/03/2018 18:44:20
 Sample Type : Unknown
 Acquired by : ezc-7
 Processed by : ezc-7

<Chromatogram>

mV



<Peak Table>

Detector A 254nm

Peak#	Ret. Time	Area	Height	Area%	Area/Height	Width at 5% Height
1	1.080	1884	293	0.011	6.424	--
2	1.219	5666	597	0.033	9.483	--
3	2.592	18464	917	0.108	20.141	--
4	3.342	66054	2203	0.388	29.986	--
5	3.505	25954	2325	0.152	11.165	--
6	3.649	18723	2490	0.110	7.520	--
7	3.757	8909	2238	0.052	3.981	--
8	3.817	57035	2232	0.335	25.552	--
9	4.538	3715	516	0.022	7.202	--
10	4.700	3808	556	0.022	6.843	--
11	4.847	8385	732	0.049	11.453	--
12	5.044	10335	1848	0.061	5.593	--
13	5.212	2791	229	0.016	12.178	--
14	5.592	1014	103	0.006	9.890	--
15	5.716	1984	328	0.012	6.049	--
16	6.353	2064	250	0.012	8.251	--
17	6.576	2660	518	0.016	5.131	--
18	6.821	38440	5760	0.226	6.673	--
19	6.927	40954	5536	0.240	7.397	--
20	7.413	24134	1746	0.142	13.824	--
21	7.922	5189	614	0.030	8.451	--
22	8.118	4609	585	0.027	7.877	--

Figure S27. HPLC trace analysis of PPSCzPN.



Elemental Analysis Service

Please send completed form and samples to:

Stephen Boyer
School of Human Sciences
Science Centre
London Metropolitan University
29 Hornsey Road
London N7 7DD

Telephone: 020 7133 3605
Fax: 020 7133 2577
Email: s.boyer@londonmet.ac.uk

Sample submitted by:	Dr Shiv Kumar
Address:	ERC Group, School of Chemistry, University of St Andrews
Telephone:	01334 467243
Email:	sk240@st-andr.ac.uk
Date Submitted:	13-02-2018

Please submit ca. 5 mg of sample.

Sample Reference No.:	SK-ITS-290118
Name of Compound:	PPSCzPN
Molecular Formula:	C ₅₆ H ₃₆ N ₄ P ₂ S ₂
Stability:	Stable at r.t. & pressure
Hazards:	None
Other Remarks:	

Element	Expected %	Found (1)	Found (2)	
Carbon	75.49	75.34	75.38	
Hydrogen	4.07	3.89	3.98	
Nitrogen	6.29	6.38	6.30	

Authorising Signature:

Date Completed:	15/02/18	Signature:	
Comments:			

Figure S28. Elemental analysis report for PPSCzPN.

—29.31

The chemical structure shows a macrocyclic molecule with a central cyanide group (C≡N). The macrocycle is composed of four repeating units, each containing a benzene ring and a carbonyl group (C=O). The units are linked by amide bonds (C(=O)-NH). The central cyanide group is coordinated to the nitrogen atoms of the amide groups, forming a central complex. The overall structure is highly symmetrical and complex.



HPLC Trace Report09May2018

<Sample Information>

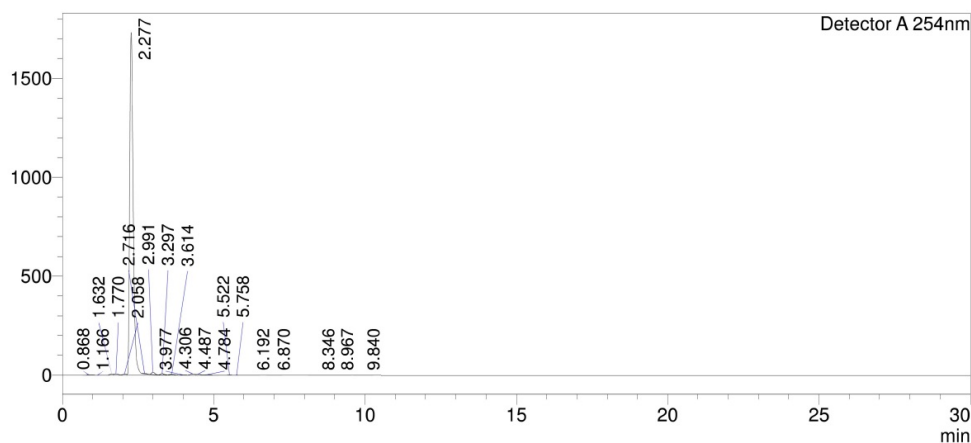
Sample Name : DiPPOCzPN-1
 Sample ID : SK-I73
 Method Filename : AcN (65).lcm
 Batch Filename : 2ndGenTADF_2.lcb
 Vial # : 1-101
 Injection Volume : 5 uL
 Date Acquired : 08/05/2018 19:55:29
 Date Processed : 08/05/2018 20:25:29

Sample Type : Unknown

Acquired by : ezc-7
 Processed by : ezc-7

<Chromatogram>

mV



<Peak Table>

Detector A 254nm

Peak#	Ret. Time	Area	Height	Area%	Area/Height	Width at 5% Height
1	0.868	22204	2023	0.151	10.973	--
2	1.166	1684	312	0.011	5.400	--
3	1.632	45734	5552	0.311	8.237	--
4	1.770	64836	6689	0.440	9.693	--
5	2.058	46989	5218	0.319	9.006	--
6	2.277	14169999	1732411	96.212	8.179	0.270
7	2.716	17563	2391	0.119	7.346	0.207
8	2.991	86545	11537	0.588	7.502	0.226
9	3.297	53430	6995	0.363	7.638	--
10	3.614	37849	3570	0.257	10.603	--
11	3.977	9647	1069	0.066	9.025	--
12	4.306	58979	5602	0.400	10.527	--
13	4.487	41923	4156	0.285	10.087	--
14	4.784	31937	2742	0.217	11.646	--
15	5.522	10647	871	0.072	12.225	--
16	5.758	8217	691	0.056	11.892	--
17	6.192	4433	492	0.030	9.018	0.304
18	6.870	1305	53	0.009	24.810	0.473
19	8.346	1339	92	0.009	14.528	--
20	8.967	9419	397	0.064	23.698	--
21	9.840	3174	199	0.022	15.942	0.519
Total		14727853	1793062	100.000		

Figure S33. HPLC trace analysis of DiPPOCzPN.

Elemental Analysis Service Request Form

Researcher name Dongyang Chen

Researcher email dc217@st-andrews.ac.uk

NOTE: Please submit ca. 10 mg of sample

Sample reference number	dc-III 14
Name of Compound	DiPPOCzPN
Molecular formula	C ₈₀ H ₅₄ N ₄ O ₄ P ₄
Stability	stable
Hazards	low hazard
Other Remarks	

Analysis type:

Single ☐ Duplicate ☒ Triplicate ☐

Analysis Result:

Element	Expected %	Found (1)	Found (2)	Found (3)
Carbon	76.31	76.37	76.55	
Hydrogen	4.32	4.30	4.37	
Nitrogen	4.45	4.66	4.53	
Oxygen				

Authorising Signature:

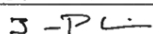
Date completed	21.05.21
Signature	
comments	

Figure S34. Elemental analysis report for DiPPOCzPN.

X-Ray Crystallography

X-ray diffraction data for compounds PPOCzPN and PPSCzPN-1 and -2 were collected at 173 K using a Rigaku MM-007HF High Brilliance RA generator/confocal optics with XtaLAB P100 diffractometer [Cu K α radiation (λ = 1.54187 Å)]. Diffraction data for PPOCICzPN were collected at 173 K using a Rigaku FR-X Ultrahigh Brilliance Microfocus RA generator/confocal optics with XtaLAB P200 diffractometer [Mo K α radiation (λ = 0.71075 Å)]. X-ray diffraction data for DiPPOCzPN were collected at 125 K using a Rigaku MM-007HF High Brilliance RA generator/confocal optics with XtaLAB P200 diffractometer [Cu K α radiation (λ =

1.54187 Å)]. Intensity data for all compounds were collected using either just ω steps, or both ω and ϕ steps, accumulating area detector images spanning at least a hemisphere of reciprocal space. Data for all compounds analysed were collected using CrystalClear¹³ and processed (including correction for Lorentz, polarization and absorption) using CrysAlisPro.¹⁴ Structures were solved by direct (SHELXS,¹⁵ SIR2004¹⁶) or dual-space (SHELXT¹⁷) methods and refined by full-matrix least-squares against F^2 (SHELXL-2018/3¹⁸). Non-hydrogen atoms were refined anisotropically, and hydrogen atoms were refined using a riding model, except for the hydrogens on water in **DiPPOCzPN** which were located from the difference Fourier map and refined isotropically subject to a distance restraint. The structure of **PPOClCzPN** showed apparent partial chloride substitution at the 6-position on both carbazole rings (approx. 15 % substitution Cl on one ring, 25% on the other), with no other differences between the two structures (Figure **S35**). The structure of **DiPPOCzPN** showed void space of 1509 Å³, containing apparent solvent molecules that could not be modelled in a chemically sensible manner. The SQUEEZE¹⁹ routine implemented in PLATON²⁰ was used to remove the contribution to the diffraction pattern of the unordered electron density in the void spaces. All calculations except SQUEEZE were performed using either the CrystalStructure²¹ or Olex2²² interface. Selected crystallographic data are presented in Table **S1**. Deposition numbers 2107137-2107141 contains the supplementary crystallographic data for this paper. These data are provided free of charge by the joint Cambridge Crystallographic Data Centre and Fachinformationszentrum Karlsruhe Access Structures service www.ccdc.cam.ac.uk/structures.

Table S1. Selected crystallographic data.

	PPOCzPN	PPOClCzPN	PPSCzPN-1	PPSCzPN-2	DiPPOCzPN
empirical formula	C ₅₆ H ₃₆ N ₄ O ₂ P ₂	C ₅₆ H _{35.6} Cl _{0.4} N ₄ O ₂ P ₂	C ₅₆ H ₃₆ N ₄ P ₂ S ₂	C ₅₇ H ₃₇ Cl ₃ N ₄ P ₂ S ₂	C ₈₀ H ₅₆ N ₄ O ₅ P ₄
fw	858.83	872.65	890.99	1010.37	1277.16
crystal description	Yellow prism	Yellow plate	Yellow needle	Yellow needle	Colourless plate
crystal size [mm ³]	0.15×0.09×0.03	0.18×0.14×0.02	0.12×0.02×0.01	0.18×0.01×0.01	0.07×0.03×0.01
space group	<i>P</i> $\bar{1}$	<i>P</i> $\bar{1}$	<i>P</i> 2 ₁ / <i>n</i>	<i>Pna</i> 2 ₁	<i>P</i> 2 ₁ / <i>n</i>
<i>a</i> [Å]	11.86946(16)	11.9815(4)	15.382(2)	31.259(2)	11.8110(2)
<i>b</i> [Å]	13.14662(19)	13.1942(4)	16.085(3)	14.5391(11)	44.7094(9)
<i>c</i> [Å]	15.46934(19)	15.4692(4)	18.243(4)	21.3955(17)	14.3862(2)
α [°]	106.2230(12)	106.482(2)			
β [°]	110.3555(12)	110.593(3)	100.705(17)		104.738(2)
γ [°]	94.7695(11)	94.306(2)			
vol [Å ³]	2128.98(5)	2153.08(13)	4435.1(14)	9723.8(12)	7346.9(2)
<i>Z</i>	2	2	4	8	4
ρ (calc) [g/cm ³]	1.340	1.346	1.334	1.380	1.155
μ [mm ⁻¹]	1.326	0.176	2.115	3.477	1.359
F(000)	892	904.8	1848	4160	2656
reflections collected	22737	28031	45516	97548	87205
independent reflections (<i>R</i> _{int})	7600 (0.0247)	9289 (0.0457)	8034 (0.4448)	16129 (0.5961)	14862 (0.0891)
parameters, restraints	577, 0	597, 2	578, 0	1225, 1	846, 2
GOF on <i>F</i> ²	1.072	1.048	0.886	0.914	1.033
<i>R</i> _I [<i>I</i> > 2σ(<i>I</i>)]	0.0367	0.0494	0.1098	0.0845	0.0501
<i>wR</i> ₂ (all data)	0.1075	0.1102	0.3739	0.2527	0.1340
largest diff. peak/hole [e/Å ³]	0.39, -0.37	0.26, -0.38	0.49, -0.71	0.30, -0.35	0.45, -0.34

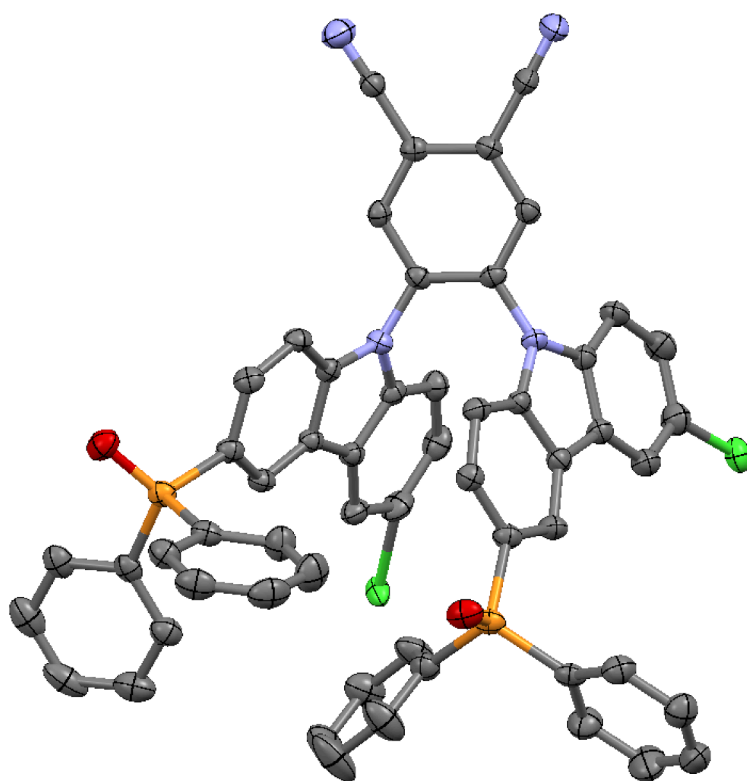


Figure S35. Thermal ellipsoid plot of the structure of **PPOClCzPN**. Ellipsoids are drawn at the 50 % probability level, hydrogen atoms are omitted, and only the chlorines are shown on the disordered sites.

Additional Electrochemical Experiments

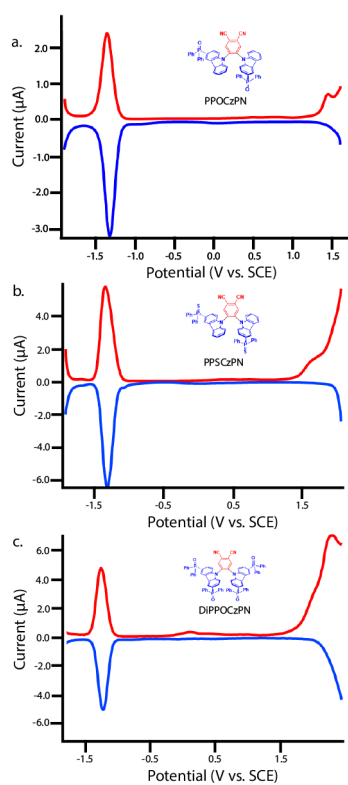


Figure S36. Differential pulse voltammograms of **PPOCzPN** (a), **PPSCzPN** (b), and **DIPPOCzPN** (c) in degassed DCM with 0.1 M $[n\text{-Bu}_4\text{N}]\text{ClO}_4$ (TBAP) as the supporting electrolyte.

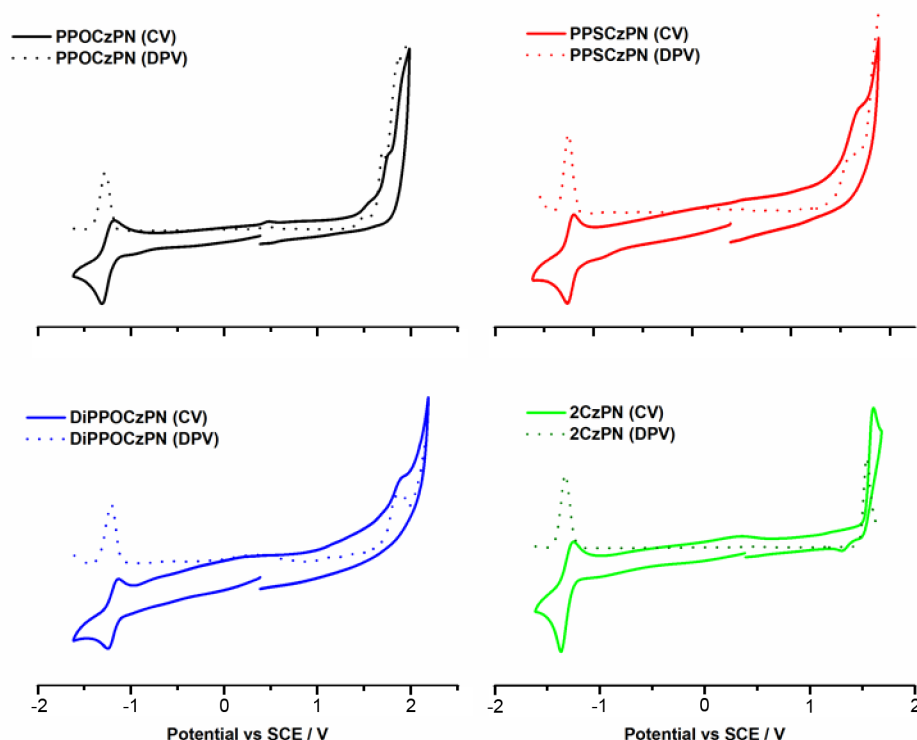


Figure S37. Cyclic voltammograms and differential pulse voltammograms (dotted) of **PPOCzPN**, **PPSCzPN**, **DiPPOCzPN** and **2CzPN** in degassed MeCN under nitrogen with 0.1 M $[n\text{-Bu}_4\text{N}]\text{PF}_6$ as the supporting electrolyte (scan rate = 100 mV s^{-1}).

Figure S37 contains an analysis of the electrochemistry occurring in MeCN to complement the electrochemical studies performed in DCM (Figure S36a-c). By the same methods, the HOMO levels of **PPOCzPN** (-6.41 eV) and **PPSCzPN** (-6.29 eV) are increasingly stabilized compared to **2CzPN** (-6.21 eV) as a result of the increased polarizability of the sulfur compared to oxygen.²³ **DiPPOCzPN** possesses the most stabilized HOMO (-6.61 eV) as a result of the introduction of the second electron-withdrawing diphenylphosphine oxide moiety. The LUMO levels lie in a narrow range of -3.43 to -3.45 eV and are close to the LUMO level of **2CzPN** (-3.38 eV), indicating very poor electronic coupling between donor and acceptor moieties.

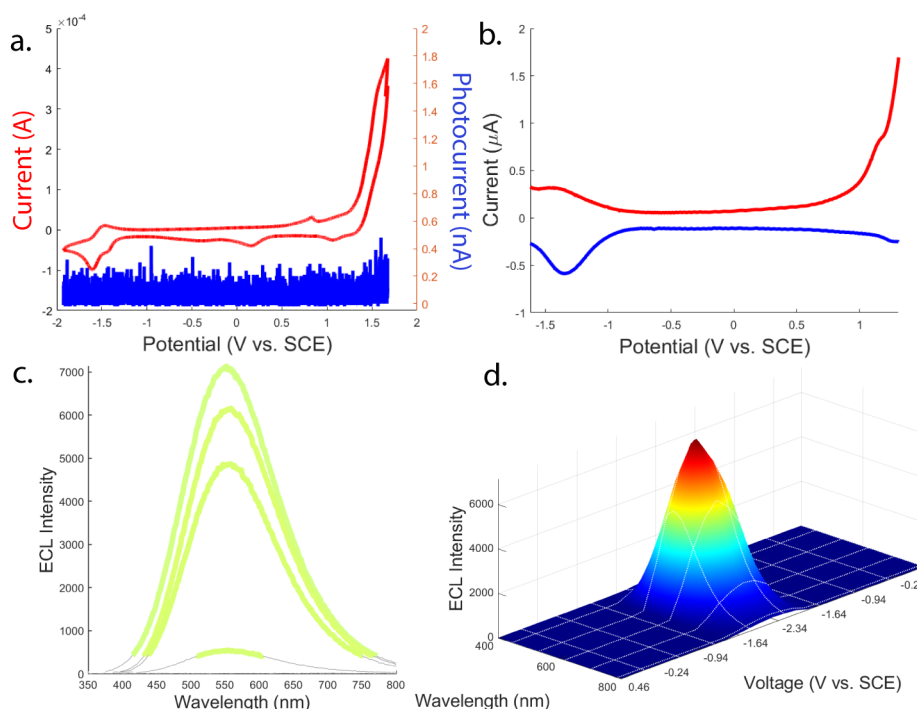


Figure S38. a. Cyclic voltammogram with current in red and photocurrent in blue (scan rate = 100 mV s^{-1}) and b. differential pulse voltammograms with the cathodic scan in blue and the anodic scan in red of $0.7 \text{ mM } 2\text{CzPN}$ in degassed DCM with $0.1 \text{ M } [n\text{-Bu}_4\text{N}]\text{ClO}_4$ (TBAP) as the supporting electrolyte. c. Spooling ECL spectroscopy of the same systems described in **Figure S38a** with an additional 20 mM BPO coreactant. The color of spectra in the inset are the individual spectrum's corresponding RGB coordinates.

2CzPN had no emission in the annihilation pathway seen in **Figure S38a**, even during 10 Hz pulsing between **2CzPN**'s first reduction and first oxidation peaks. Unfortunately, this lack of emission prevented the measurement of **2CzPN**'s ECL emission delays after excitation. However, upon addition of 20 mM BPO **2CzPN** brightly fluoresced with a constant central peak of 550 nm in **Figure S38c**. This 550 nm wavelength is the same wavelength emitted by **DiPPOCzPN** in the same BPO conditions and is red-shifted 50 nm from the **2CzPN** PL studies. This wavelength does not match any other wavelengths in this study and is the most red-shifted of all emission wavelengths.

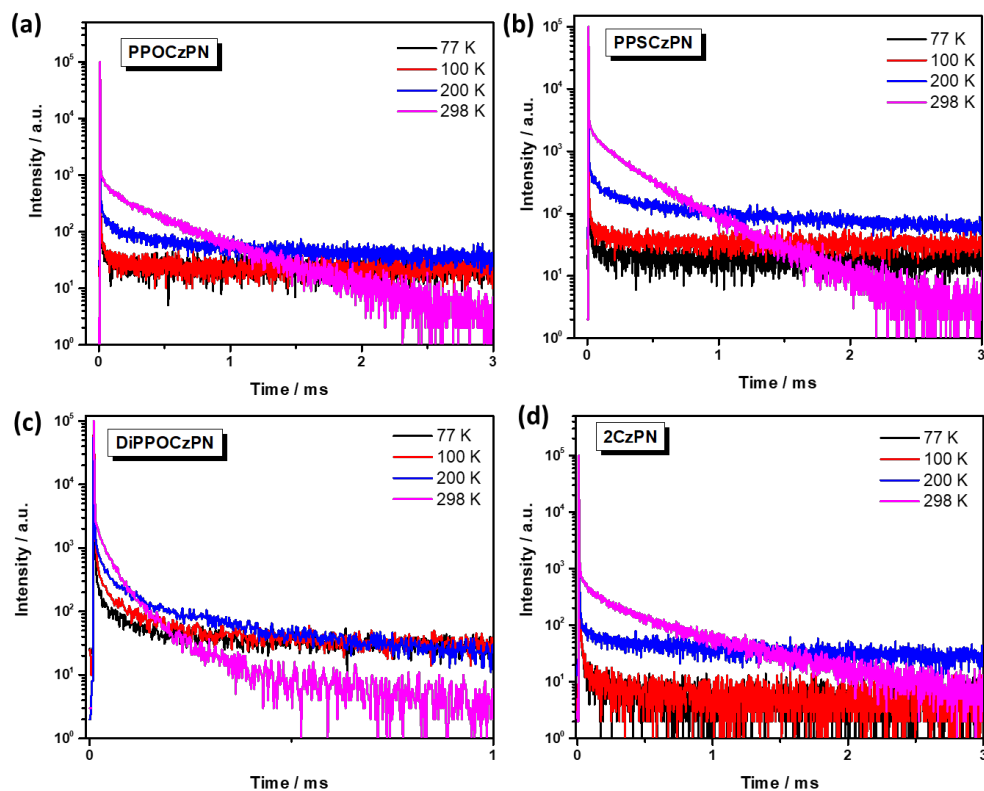


Figure S39. Temperature-dependent time-resolved emission decay profile in 10 wt% mCP doped thin films: (a) PPOCzPN, (b) PPSCzPN, (c) DiPPOCzPN, and (d) 2CzPN ($\lambda_{\text{exc}} = 378$ nm).

Theoretical modelling

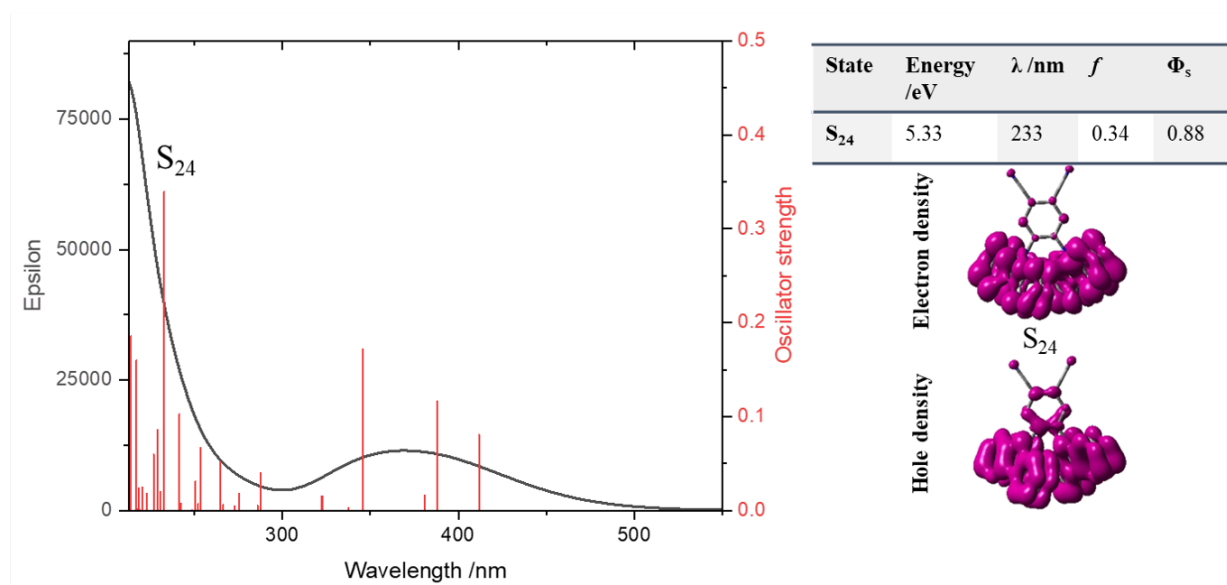
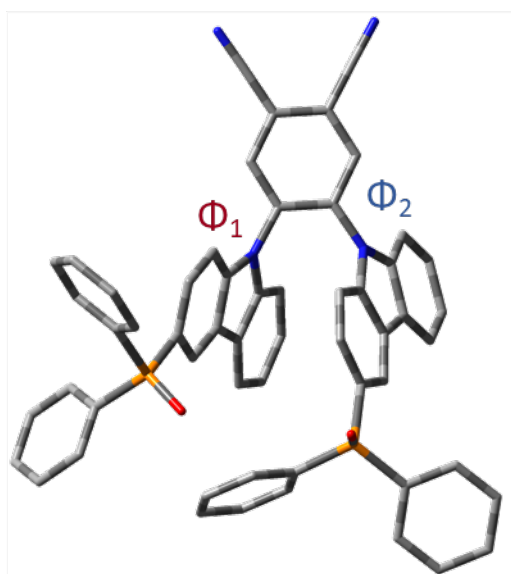
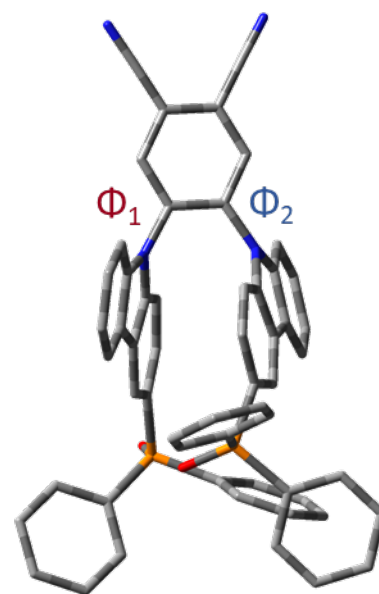


Figure S40. Theoretical absorption spectrum of **2CzPN** obtained at the TDA-PBE0/6-31G(d,p) level of theory in gas phase as well as the hole and electron densities related to S_{24} state and its photophysical properties.

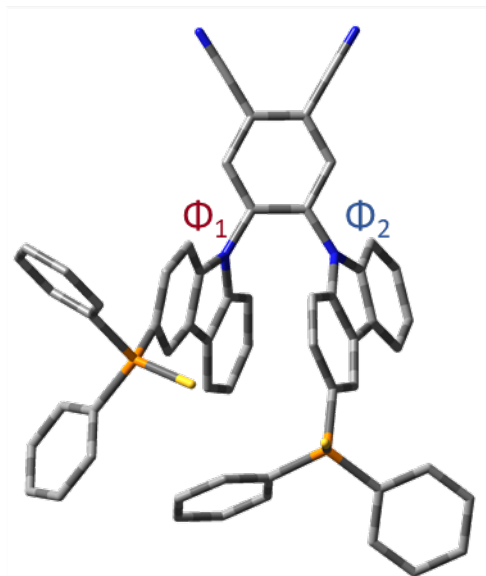


Rotamer 1

PPOCzPN

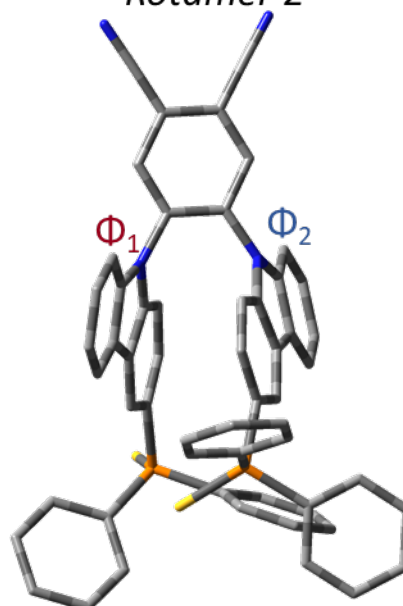


Rotamer 2



Rotamer 1

PPSCzPN



Rotamer 2

Figure S41. Structures of the two rotamers of **PPOCzPN** and **PPSCzPN**

Table S2. Calculated HOMO and LUMO energies of the less stable rotamer of PPOCzPN and PPSCzPN obtained at the PBE0/6-31G(d,p) level of theory in gas phase versus MeCN.

	In gas phase			In MeCN		
	HOMO /eV	LUMO /eV	ΔE /eV	HOMO /eV	LUMO /eV	ΔE /eV
PPOCzPN rotamer 1	-6.23	-2.57	3.66	-6.17	-2.50	3.67
PPSCzPN rotamer 1	-5.82	-2.57	3.25	-6.17	-2.50	3.67

Table S3. Calculated excitation energies, ΔE_{ST} , oscillator strengths, and main component of the excitations in terms of one-electron transitions for the three compounds obtained in gas phase at the TDA-PBE0/6-31G(d,p) level of theory.

Compound	States	Energy /eV	f	Main component of the excitation		ϕ_s
PPOCzPN	T ₁	2.62	0.021	HOMO-2	→ LUMO	0.58
	S ₁	2.82		HOMO → LUMO (97.5%)		0.34
	ΔE_{ST}	0.20				
PPSCzPN	T ₁	2.63	0.022	HOMO-2	→ LUMO	0.59
	S ₁	2.84		HOMO-2 → LUMO (96.6%)		0.35
	ΔE_{ST}	0.21				
DiPPOCzPN	T ₁	2.71	0.038	HOMO → LUMO (85.0%)		0.64
	T ₂	2.96				0.49
	S ₁	2.97		HOMO → LUMO (97.5%)		0.39

Table S4. Calculated excitation energies, ΔE_{ST} , oscillator strengths, and main component of the excitations in terms of one-electron transitions for the less stable rotamer obtained in gas phase at the TDA-PBE0/6-31G(d,p) level of theory.

Compound	States	Energy /eV	f	Main component of the excitation	ϕ_s
PPOCzPN Rotamer 1	T ₁	2.68		HOMO → LUMO (78.0%)	0.64
	T ₂	2.93			0.51
	S ₁	2.95	0.049	HOMO → LUMO (98.2%)	0.38
	ΔE_{ST}	0.27			
PPSCzPN Rotamer 1	T ₁	2.66		HOMO-2 → LUMO (38.9%)	0.59
	S ₁	2.81	0.014	HOMO-2 → LUMO (84.6%)	0.22
	ΔE_{ST}	0.15			

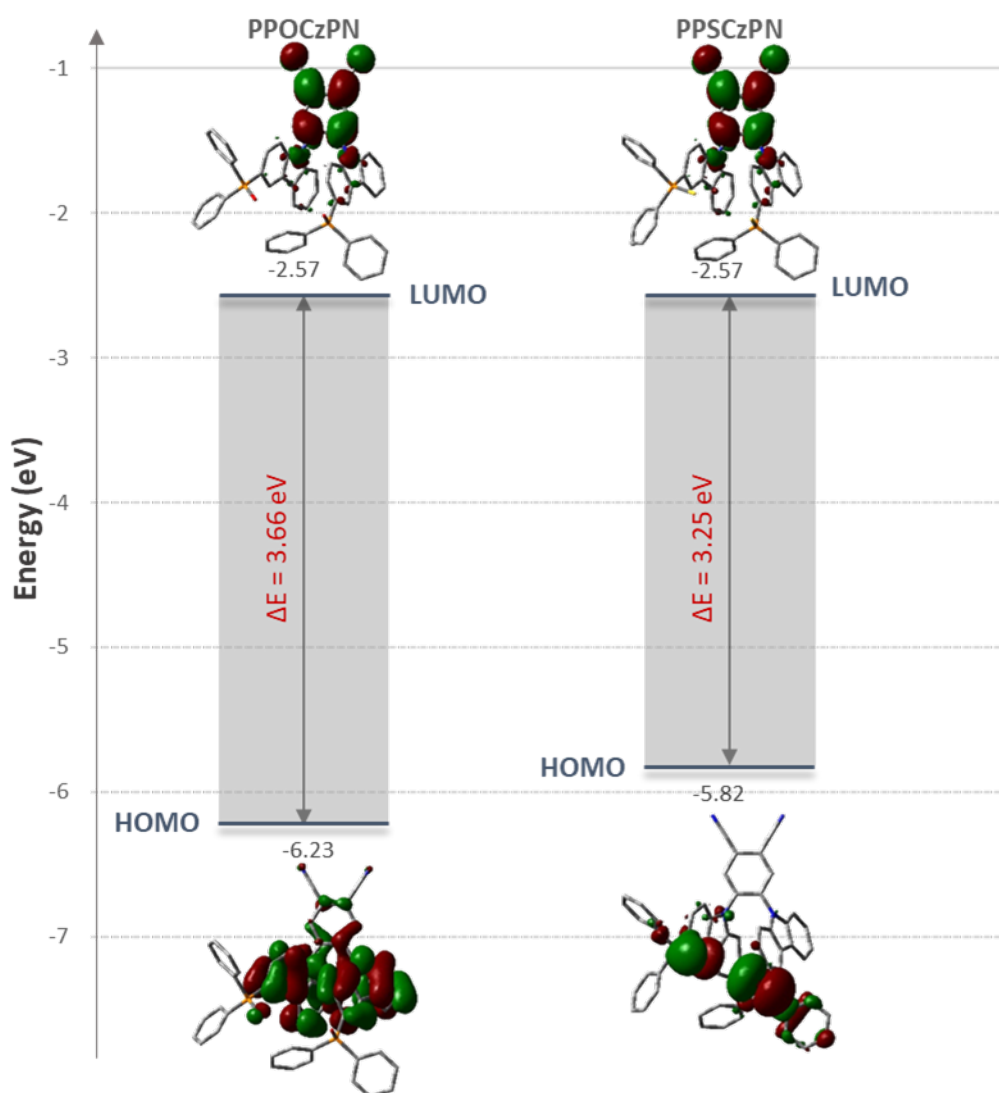


Figure S42. Shape of the HOMO and LUMO levels in rotamer 1 of **PPOCzPN** and **PPSCzPN** obtained in gas phase at the PBE0/6-31G(d,p) level of theory.

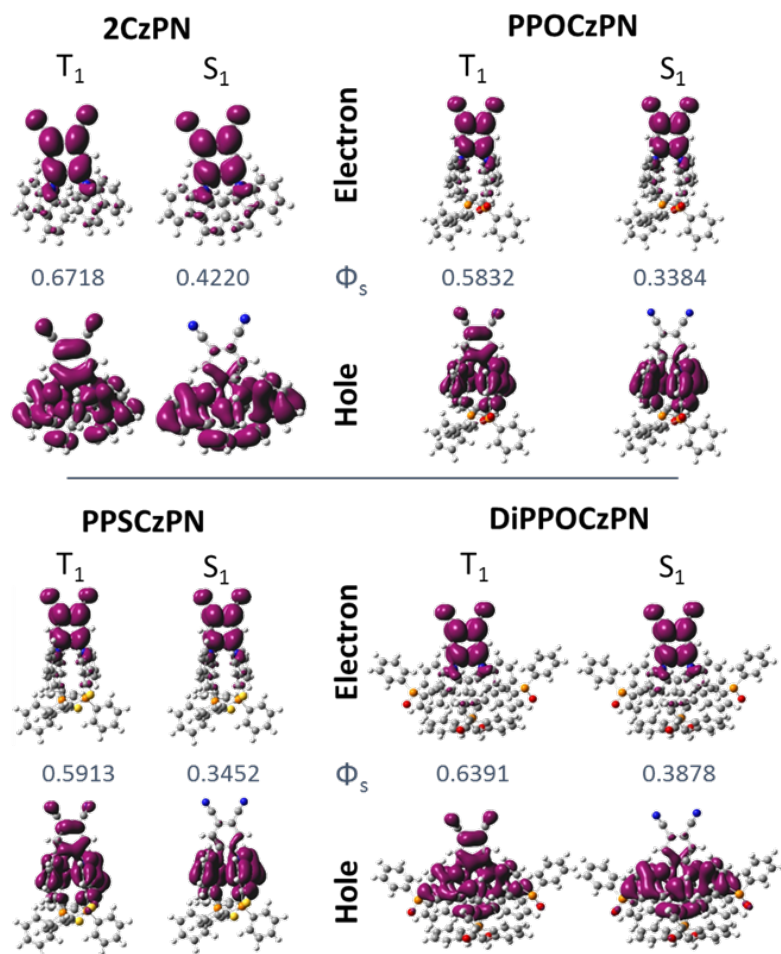


Figure S43. Representations of hole detachment and electron attachment densities for 2CzPN and its derivatives in the gas phase.

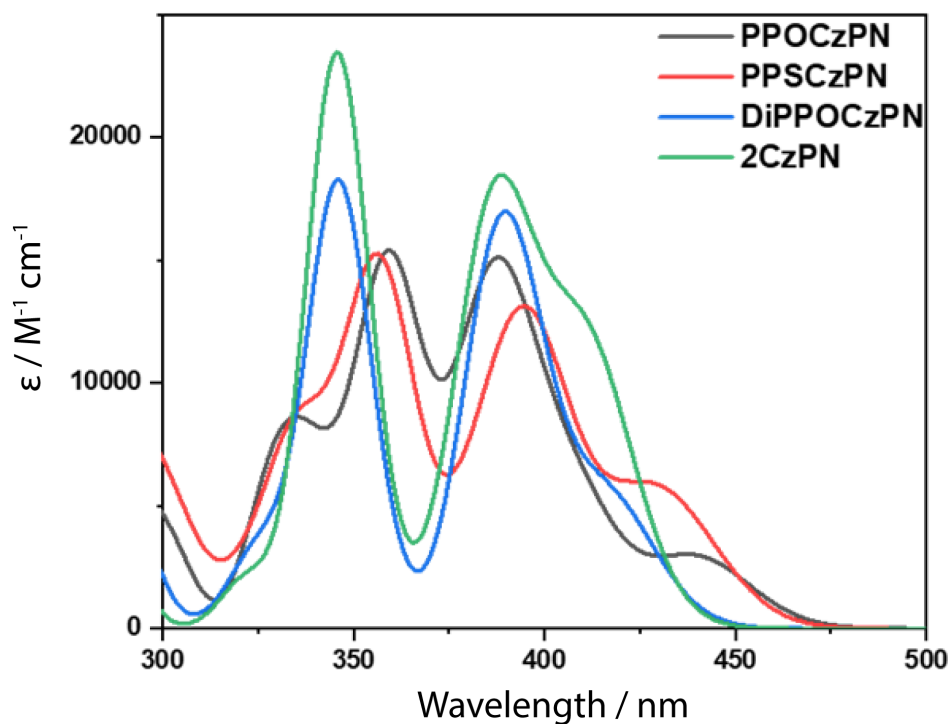


Figure S44. Theoretical absorption spectra of **2CzPN** and its derivatives simulated in the gas phase.

Table S5. TD-DFT calculated energies of the S_1 and T_1 excited states in gas phase versus toluene and acetonitrile for vertical excitation processes.

Emitter	Gas	Toluene	Acetonitrile
PPOCzPN	T₁	2.62	2.60
	S₁	2.82	2.79
PPSCzPN	T₁	2.63	2.63
	S₁	2.84	2.83
DiPPOCzPN	T₁	2.71	2.72
	S₁	2.97	2.97
2CzPN	T₁	2.67	2.63
	S₁	3.01	2.94

Electrochemiluminescence

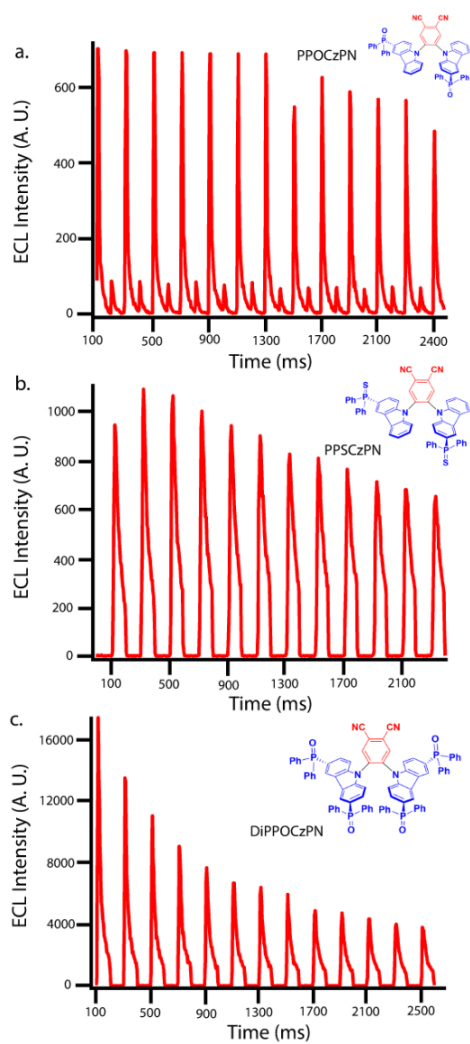


Figure S45. Extended annihilation pulsing spectra of **PPOCzPN**, **PPSCzPN** and **DiPPOCzPN** in degassed DCM with 0.1 M of TBAP.

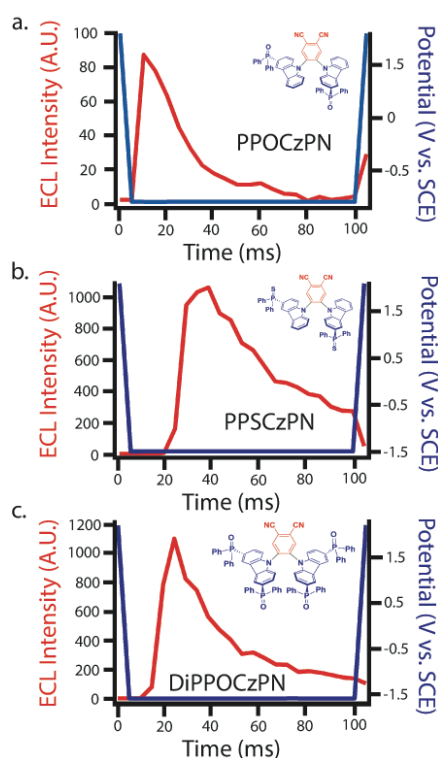


Figure S46. Zoomed annihilation pulsing spectra of **PPOCzPN**, **PPSCzPN** and **DiPPOCzPN** in degassed DCM with 0.1 M of TBAP.

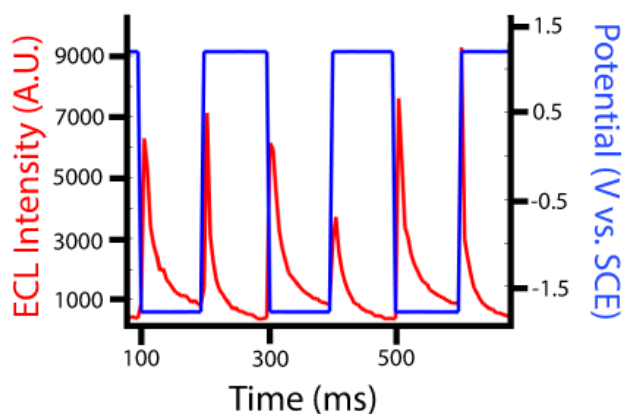


Figure S47. Annihilation pulsing for 0.7 mM **Ru(bpy)₃(PF₆)₂** in degassed DCM with 0.1 M TBAP as an electrolyte.

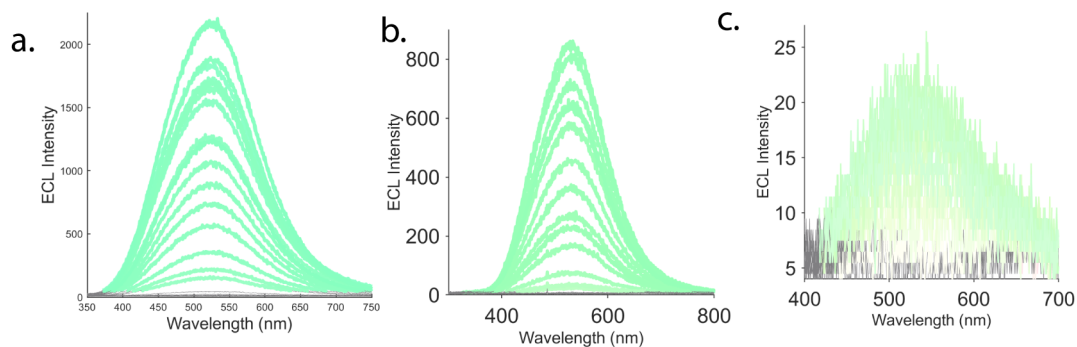


Figure S48. A zoom-in of respective insets of **Figure 8d-f**. The color of spectra in the inset are the individual spectrum's corresponding RGB coordinates.

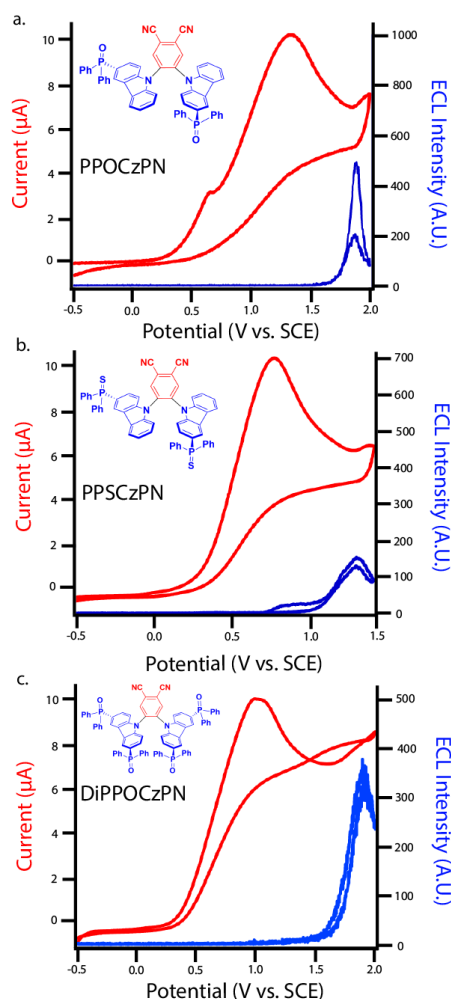


Figure S49. CVs (red) along with ECL-voltage curves (blue) during potential pulsing at a pulsing frequency of 10 Hz for **PPOCzPN**, **PPSCzPN** and **DiPPOCzPN**, (a-c, respectively), all with 5 mM TPrA added as a co-reactant.

In **Figure S48**, 5 mM TPrA was added to the electrochemical systems described in **Figure 3a-c**. Around 0.35 V vs. Fc, TPrA is reduced and ultimately turns into TPrA[•]. When **PPOCzPN**, **PPSCzPN** and **DiPPOCzPN** are oxidized to form **PPOCzPN^{•+}**, **PPSCzPN^{•+}** and **DiPPOCzPN^{•+}**, TPrA[•] can donate an electron to the LUMOs of oxidized compounds to produce **PPOCzPN^{*}**, **PPSCzPN^{*}** and **DiPPOCzPN^{*}** excited states, respectively. **PPOCzPN^{*}**, **PPSCzPN^{*}** and **DiPPOCzPN^{*}** can then emit light. Furthermore, TPrA[•]/TPrA has an oxidation potential of 1.70 ± 0.1 V from previous studies potentially allowing TPrA[•] to reduce of the compounds.²⁴ The most negative redox couple in this study **PPSCzPN/PPSCzPN^{•-}**, was found to be -1.83 V placing itself on the upper range of the TPrA oxidation potential of 1.80 V.

In fact, **PPSCzPN** produced photocurrent with TPrA despite the high reduction potential of **PPSCzPN^{•-}**. The ECL maximum emission and ECL efficiencies for **PPOCzPN**, **PPSCzPN** and **DiPPOCzPN** were measured at 490, 150 and 360 nA and 7.3, 1.0 and 3.0%, respectively. Similar to the BPO co-reactant systems, **PPOCzPN** had the highest maximum ECL emissions and efficiency. The relative intensities are vastly different than the BPO co-reactant systems. **PPOCzPN**'s TPrA ECL efficiency is only double that of **DiPPOCzPN** instead of 30 times for the BPO ECL efficiency,

further indicating that **DiPPOCzPN** exhibited some form of quenching with BPO as co-reactant. **PPSCzPN**'s ECL efficiency is 7 times weaker than **PPOCzPN**'s, instead of 3 times weaker in the BPO system, suggesting it is exhibiting some sort of quenching in the TPrA co-reactant pathway. **PPOCzPN**^{•+} also exhibited the highest reactivity towards TPrA, generating the highest ECL efficiency and further proving its suitability as an OLED luminophore.

Interestingly, **PPSCzPN** showed two ECL waves, with one starting at ~1.1 V and another starting roughly at ~1.6 V seen in **Figure S49b**. This first wave has been thoroughly studied in a Ru(bpy)₃²⁺/TPrA system by Bard et al.²⁵ Briefly, Bard et al. attributed the first wave to TPrA acting as both the reductant and oxidant forming Ru(bpy)₃⁺ and Ru(bpy)₃^{2+•} respectively and the second wave the typical ECL pathway discussed already. In this study, TPrA[•] reduces **PPSCzPN** to **PPSCzPN**^{•-}, then TPrA^{•+} may oxidize **PPSCzPN**^{•-} into **PPSCzPN**^{*} which can subsequently emit light. Furthermore, the TPrA^{•+}/TPrA redox couple was previously found to be 0.95 V where TPrA^{•+} has a half-life of ~0.2 ms permitting this persistent radical to oxidize **PPSCzPN**^{•-}, ultimately producing weak ECL (**Figure S49**).²⁵ In fact, **PPSCzPN** had the lowest oxidation potential out of all the compounds in this study, allowing this ECL pathway to only be seen for **PPSCzPN**.

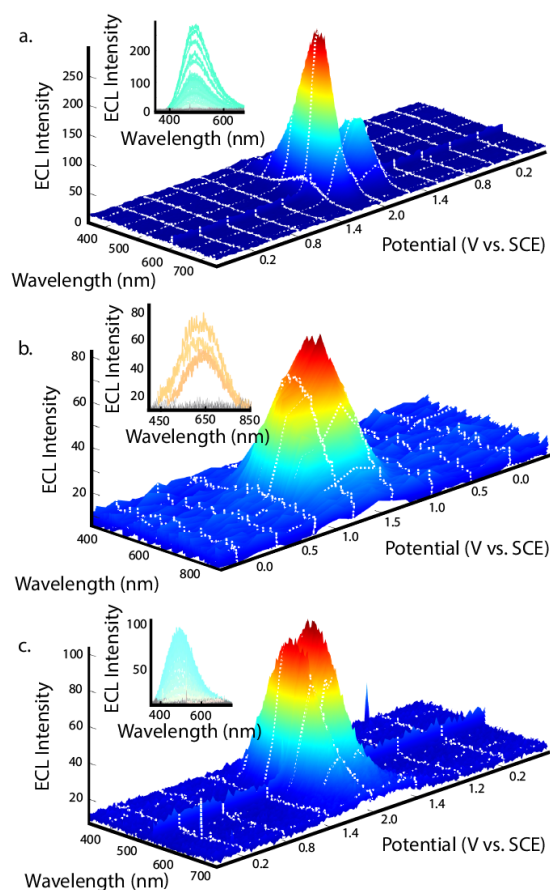


Figure S50. Spooling ECL spectroscopy of the same systems described in **Figure S47**. Insets of each figure represent the respective spectra rotated to view a 2D wavelength versus ECL intensity. The color of spectra in the inset are the individual spectrum's corresponding RGB coordinates.

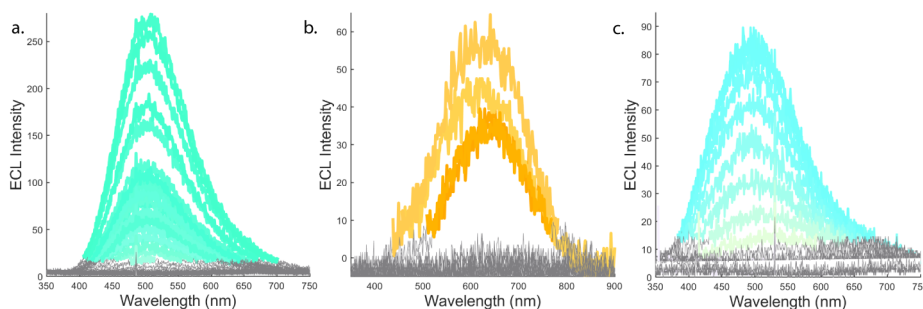


Figure S51. A zoom-in of respective insets of **Figure S50**. The color of spectra in the are the observable individual spectrum's corresponding RGB coordinates.

Figure S50 show the TPrA co-reactant systems with the zoom-in of insets seen in Figure S51, which vary in color more than the BPO co-reactant systems. **PPOCzPN** has a similar green emission to the BPO emissions with CIE coordinates of (0.27, 0.37). The emission for the **PPSCzPN**/TPrA is drastically red shifted compared to those of the other emitters in Figure S50b, with an orange emission with CIE coordinates of (0.43, 0.41). In the inset of Figure S50b, the emission color changes to a lighter orange color as the overpotential is increased and returns to the original color when decreasing

the potential. The peak wavelength shifts from 650 to 620 nm and the CIE coordinates shift from (0.45, 0.40) to (0.42, 0.41) with increasing overpotential. In fact, excimer formation was not seen in the BPO or annihilation ECL pathways for **PPSCzPN**. Furthermore, spooling spectroscopy suggests **PPSCzPN*** forms an excimer with **PPSCzPN**⁺ where the degree of red shifting decreases with increased **PPSCzPN**⁺ concentration in the vicinity of the electrode. Unfortunately, spooling spectroscopy elucidated only the second ECL wave for the **PPSCzPN**/TPrA system seen in Figure **S50b** due to the sensitivity differences between the PMT and CCD camera. **DiPPOCzPN** in Figure **S51c** has the bluest emission of all ECL species with constant CIE coordinates of (0.27, 0.34). This blue emission seems to be closely related to **DiPPOCzPN**'s PL wavelength seen, indicating corresponding emission origins.

References

1. Wong, M. Y.; Hedley, G. J.; Xie, G.; Kölln, L. S.; Samuel, I. D. W.; Pertegás, A.; Bolink, H. J.; Zysman-Colman, E., Light-Emitting Electrochemical Cells and Solution-Processed Organic Light-Emitting Diodes Using Small Molecule Organic xThermally Activated Delayed Fluorescence Emitters. *Chem. Mater.* **2015**, 27 (19), 6535-6542.
2. Demas, J. N.; Crosby, G. A., The Measurement of Photoluminescence Quantum Yields. A Review. *J. Phys. Chem.* **1971**, 75 (8), 991-1024.
3. Melhuish, W. H., QUANTUM EFFICIENCIES OF FLUORESCENCE OF ORGANIC SUBSTANCES: EFFECT OF SOLVENT AND CONCENTRATION OF THE FLUORESCENT SOLUTE1. *J. Phys. Chem.* **1961**, 65 (2), 229-235.
4. Adsetts, J.; Zhang, R.; Yang, L.; Chu, K.; Wong, J.; Love, D. A.; Ding, Z., Efficient White Electrochemiluminescent Emission from Carbon Quantum Dot Films. *Front. Chem.* **2020**, 8, 865-878.
5. Faulkner, L. R.; Tachikawa, H.; Bard, A. J., Electrogenerated Chemiluminescence. VII. The Influence of an External Magnetic Field on Luminescence Intensity. *J. Am. Chem. Soc.* **1972**, 94 (3), 691-699.
6. Frisch, M. J.; Trucks, G. W.; Schlegel, H. B.; Scuseria, G. E.; Robb, M. A.; Cheeseman, J. R.; Scalmani, G.; Barone, V.; Mennucci, B.; Petersson, G. A.; Nakatsuji, H.; Caricato, M.; Li, X.; Hratchian, H. P.; Izmaylov, A. F.; Bloino, J.; Zheng, G.; Sonnenberg, J. L.; Hada, M.; Ehara, M.; Toyota, K.; Fukuda, R.; Hasegawa, J.; Ishida, M.; Nakajima, T.; Honda, Y.; Kitao, O.; Nakai, H.; Vreven, T.; Montgomery Jr., J. A.; Peralta, J. E.; Ogliaro, F.; Bearpark, M. J.; Heyd, J.; Brothers, E. N.; Kudin, K. N.; Staroverov, V. N.; Kobayashi, R.; Normand, J.; Raghavachari, K.; Rendell, A. P.;

- Burant, J. C.; Iyengar, S. S.; Tomasi, J.; Cossi, M.; Rega, N.; Millam, N. J.; Klene, M.; Knox, J. E.; Cross, J. B.; Bakken, V.; Adamo, C.; Jaramillo, J.; Gomperts, R.; Stratmann, R. E.; Yazyev, O.; Austin, A. J.; Cammi, R.; Pomelli, C.; Ochterski, J. W.; Martin, R. L.; Morokuma, K.; Zakrzewski, V. G.; Voth, G. A.; Salvador, P.; Dannenberg, J. J.; Dapprich, S.; Daniels, A. D.; Farkas, Ö.; Foresman, J. B.; Ortiz, J. V.; Cioslowski, J.; Fox, D. J. *Gaussian 16 Rev. A.03*, Gaussian, Inc.: Wallingford, CT, USA, 2016.
7. Adamo, C.; Barone, V., Toward reliable density functional methods without adjustable parameters: The PBE0 model. *J. Chem. Phys.* **1999**, *110* (13), 6158-6170.
 8. Hirata, S.; Head-Gordon, M., Time-dependent density functional theory within the Tamm–Dancoff approximation. *Chem. Phys. Lett.* **1999**, *314* (3), 291-299.
 9. Dreuw, A.; Head-Gordon, M., Single-Reference ab Initio Methods for the Calculation of Excited States of Large Molecules. *Chem. Rev.* **2005**, *105*, 4009-4037.
 10. Etienne, T.; Assfeld, X.; Monari, A., New Insight into the Topology of Excited States through Detachment/Attachment Density Matrices-Based Centroids of Charge. *J Chem Theory Comput* **2014**, *10* (9), 3906-14.
 11. Mennucci, B., Polarizable continuum model. *WIREs Computational Molecular Science* **2012**, *2* (3), 386-404.
 12. Dennington, R.; Keith, T.; Millam, J. M. GaussView, Version 5.0.8. 2009.
 13. *CrystalClear-SM Expert v2.1*; Rigaku Americas, *The Woodlands, Texas, USA* and Rigaku Corporation, *Tokyo, Japan*, 2015.
 14. *CrysAlisPro*, v1.171.38.46-v1.171.40.40a; Rigaku Oxford Diffraction, Rigaku Corporation, *Oxford, U.K.*, 2015-2019.
 15. Sheldrick, G. M., A short history of SHELX. *Acta Crystallogr., Sect. A: Found. Crystallogr.* **2008**, *64* (1), 112-122.
 16. Burla, M. C.; Caliendo, R.; Camalli, M.; Carrozzini, B.; Cascarano, G. L.; De Caro, L.; Giacovazzo, C.; Polidori, G.; Spagna, R., SIR2004: an improved tool for crystal structure determination and refinement. *J. Appl. Crystallogr.* **2005**, *38* (2), 381-388.
 17. Sheldrick, G. M., SHELXT–Integrated space-group and crystal-structure determination. *Acta Crystallogr., Sect. A* **2015**, *71* (1), 3-8.
 18. Sheldrick, G. M., Crystal structure refinement with SHELXL. *Acta Crystallogr., Sect. C* **2015**, *71* (1), 3-8.

19. Spek, A. L., PLATON SQUEEZE: a tool for the calculation of the disordered solvent contribution to the calculated structure factors. *Acta Crystallogr., Sect. C* **2015**, 71 (1), 9-18.
20. Spek, A. L., Structure validation in chemical crystallography. *Acta Crystallogr., Sect. D* **2009**, 65 (2), 148-155.
21. *CrystalStructure*, v4.3.0; Rigaku Americas, *The Woodlands, Texas, USA*, and Rigaku Corporation, *Tokyo, Japan*, 2018.
22. Dolomanov, O. V.; Bourhis, L. J.; Gildea, R. J.; Howard, J. A.; Puschmann, H., OLEX2: a complete structure solution, refinement and analysis program. *J. Appl. Crystallogr.* **2009**, 42 (2), 339-341.
23. Li, J.; Ding, D.; Tao, Y.; Wei, Y.; Chen, R.; Xie, L.; Huang, W.; Xu, H., A Significantly Twisted Spirocyclic Phosphine Oxide as a Universal Host for High - Efficiency Full - Color Thermally Activated Delayed Fluorescence Diodes. *Adv. Mater.* **2016**, 28 (16), 3122-3130.
24. Lai, R. Y.; Bard, A. J., Electrogenenerated chemiluminescence. 70. The application of ECL to determine electrode potentials of tri-n-propylamine, its radical cation, and intermediate free radical in MeCN/benzene solutions. *J. Phys. Chem. A* **2003**, 107 (18), 3335-3340.
25. Miao, W.; Choi, J.-P.; Bard, A. J., Electrogenenerated chemiluminescence 69: The Tris (2, 2 '-bipyridine) ruthenium (II),(Ru (bpy) 3^{2+})/Tri-n-propylamine (TPrA) system revisited A new route involving TPrA \bullet^{+} Cation Radicals. *J Am. Chem. Soc.* **2002**, 124 (48), 14478-14485.